UNIVERSITE JOSEPH KI-ZERBO

ECOLE DOCTORALE INFORMATIQUE ET CHANGEMENTS CLIMATIQUES

BURKINA FASO

Unité-Progrès-Justice

MASTER RESEARCH PROGRAM

SPECIALITY: INFORMATICS FOR CLIMATE CHANGE (ICC)

MASTER THESIS

Subject:

Using model based AI to improve operational predictability of heat waves in developing countries: case study of Abidjan.

Presented on the 20th July and by:

GADOU Dedi Yoris Etienne

Major Supervisor

Dr. Ousmane COULIBALY
Associate professor
at Université Joseph KI-ZERBO

Co-Supervisor

Dr. Maurin Pierre Natanael ZOUZOUA
Chercheur Postdoctoral au Laboratoire Atmospheres, Milieux et Observation Spatiales (LATMOS)

Academic year 2022-2023

Dedication

With profound gratitude, I dedicate this work to GOD, whose divine presence has filled my heart and mind throughout this endeavor. I extend my heartfelt dedication to my beloved Father and Mother, whose unwavering love, sacrifice, and encouragement have been my pillars of strength.

Acknowledgments

First and foremost, I am deeply thankful to the Federal Ministry of Education and Research (BMBF) and the West African Science Service Centre on Climate Change and Adapted Land Use (Wascal) for granting me the scholarship that made this research possible. Their financial assistance and belief in my potential have been instrumental in pursuing my academic and professional goals. I extend my heartfelt appreciation to Professor Tanga Pierre ZOUNGRANA, the Director of "Ecole Doctoral Informatique et Changement Climatique" (ED-ICC), to Dr. Ousmane COULIBALY, the Deputy Director of ED-ICC, to Dr. Benewindé Jean-Bosco ZOUNGRANA, the scientific coordinator, and all the administrative staff of ED-ICC, for the implementation of the educational and social activities. I am deeply grateful to Dr. Ousmane COULIBALY for accepting the role of my Major Supervisor. His expertise, guidance, and valuable insights have been crucial in shaping the methodology and analysis of my research. I would also like to acknowledge Dr Maurin Pierre Natanael ZOUZOUA for serving as my Co-supervisor and providing valuable inputs and feedback throughout the research process. I would like to express my sincere appreciation to the members of the jury who will evaluate and provided valuable feedback on my research. Their expertise and insights have contributed significantly to the improvement and validation of my work. I would like to extend my gratitude to Benjamin Aristide AGUIA, my internship supervisor at SODEXAM. His guidance, mentorship, and support during the internship period have been instrumental in gaining practical insights and enhancing my research skills. I extend my heartfelt gratitude to the professors and individuals whose writings, advice, and criticism have guided and influenced my reflections. I would also like to express my deep appreciation and gratitude to my family for their unwavering love, support, and understanding throughout my academic journey. Their constant encouragement, belief in my abilities, and sacrifices have been the base of my achievements. I would like to express my gratitude to the senior members from the first and second batch of EDICC Ouaga. I am thankful to all those who, whether near or far, directly or indirectly, played a role in facilitating and making these studies a reality.

Abstract

Heat waves (HW) pose significant threats as deadly natural disasters, leading to human casualties and crop damage. The warming trend attributed to climate change is particularly affecting tropical Africa, with further temperature increases expected in the future. Consequently, HW events are projected to become more frequent in this region. This study first provides a temporal investigation of HW occurrences in Abidjan from 2009 to 2022, shedding light on its trend during these past years. In this work, an approach is proposed to predict HWs over Abidjan. The approach is based on a deep learning (DL) model that is optimized through Bayesian optimization and trained with the fifth generation of European ReAnalysis (ERA5) and historical data from the Abidjan synoptic station. Furthermore, because of the scarcity of this event caused by its unusual occurrence, the proposed approach leverages the advantages of transfer learning (TL) and random under-sampling (RUS) techniques to effectively address the challenge of class imbalance in the available data. The model demonstrates a remarkable performance which is supported by an AUC metric value of 99.4% for a RUS rate of 0.25% indicating high discriminatory power and predictive accuracy. This study gives important insights into HW prediction in West African capitals and highlights the effectiveness of artificial neural networks (ANNs) for effective mitigation of socio-economic impacts.

Keywords: Heat wave, Climate change, Deep learning, class imbalance, prediction, Abidjan

Résumé

Les vagues de chaleur (HW) constituent une menace importante en tant que catastrophes naturelles mortelles, entraînant des pertes humaines et des dommages aux cultures. La tendance au réchauffement attribuée au changement climatique affecte particulièrement l'Afrique tropicale, et des hausses de température sont prévues à l'avenir. Par conséquent, les HW devraient devenir plus fréquentes dans cette région. Cette étude fournit d'abord une étude temporelle des occurrences de HW à Abidjan de 2009 à 2022, mettant en lumière sa tendance au cours de ces dernières années. Dans cette étude, une approche est proposée pour prédire les HW sur Abidjan. Après quoi, une approche est proposée pour la prédiction des vagues de chaleur sur Abidjan. Cette approche repose sur l'utilisation d'un modèle d'apprentissage profond obtenu par application de l'optimisation bayésienne. Le modèle est entraîné en utilisant les données ERA5 ainsi que les données historiques de la station synoptique d'Abidjan. En raison de la rareté des vagues de chaleur, l'approche proposée exploite les avantages des techniques d'apprentissage par transfert et de RUS pour relever efficacement le défi du déséquilibre des classes dans les données disponibles. Le modèle démontre une performance remarquable qui est soutenue par une valeur de la métrique AUC de 99,4 % pour un taux de RUS de 0,25 % indiquant un pouvoir discriminatoire et une précision prédictive élevés. Cette étude donne un aperçu important sur la prévision des HW dans les capitales de l'Afrique de l'Ouest et souligne l'efficacité des réseaux de neuronaux artificiels (ANN) pour l'atténuation effective des impacts socio-économiques.

Mots-clés: Vague de chaleur, changement climatique, apprentissage profond, déséquilibre des classes, prédiction, Abidjan.

List of tables

List of figures

Acronyms and abbreviations

AI: Artificial Intelligence

ANN: Artificial Neural Network

AT: Apparent Temperature

CMIP5: Coupled Model Intercomparison Project Phase 5

CORDEX: COordinated Regional Downscaling Experiment

DL: Deep Learning

DNN: Deep Neural Network

ERA5: the fifth generation of European ReAnalysis

GAM: Generalized Additive Model

GCM: General Circulation Model

HI: Heat Index

HW: Heat wave

HWDI: Heat Wave Duration Index

HWMI: Heat Wave Magnitude Index

HWPP: Heat Waves per Period

IPCC: Intergovernmental Panel on Climate Change

MI: Meteorological Indicator

ML: Machine Learning

NET: Net Effective Temperature

PCM: Parallel Climate Model

RCP: Representative Concentration Pathway

RH: Relative humidity

TL: Transfer learning

UTCI: Universal Thermal Climate Index

WBGT: Wet-Bulb Globe Temperature

WBT: Wet-Bulb Temperature

RUS: Ramdom Undersampling Sampling

AUC: Area Under the Curve

CNN: Convolutional Neural Network

Introduction

1.Problem statement

Climate extremes are a topic of tremendous interest around the world because of the significant monetary, human, and physical consequences (Coumou & Rahmstorf, 2012). Global warming leads to the rise of extreme events and reinforces their intensity (Engdaw et al., 2022; Fischer & Schär, 2010). In its fifth assessment report, the Intergovernmental Panel on Climate Change (IPCC) affirmed that human activities have been the primary cause of observed shifts in various weather and climate extremes dating back to around 1950. Human activities, especially the burning of fossil fuels in energy production, industry, agriculture, and related industries, have led to the discharge of significant amounts of greenhouse gases (carbon dioxide, methane, nitrous oxide, etc.) into the Earth's atmosphere. This leads to an overall increase in the Earth's average atmospheric temperature, thereby causing global warming and related climate change (Melillo et al., 2014). These changes cause more frequent occurrences of HW and extreme precipitation in diverse regions (Meyer et al., 2015). HWs are one of the deadliest natural disasters, as they can cause human casualties and crop damage (Fouillet et al., 2006; Michelozzi et al., 2009; Shaposhnikov et al., 2014; Stafoggia et al., 2006; Sung et al., 2013). Tropical Africa is experiencing warming as a result of climate change, and temperature is expected to further increase in the future (IPCC, 2014; Sylla et al., 2016).

Thus, HW events are expected to become more frequent in tropical Africa (Giorgi et al., 2014; Liu et al., 2017; Russo et al., 2014). A thorough analysis undertaken by Campbell et al. (2018) revealed that underdeveloped countries may face the most extreme HWs in the future, in addition to the instability of their economy. According to Engdaw et al. (2022), temperature increase and HWs are likely to raise the cost of energy in the future, exacerbating the socioeconomic issues encountered in Sub-Saharan Africa, where most of the population currently lacks access to electricity.

Moreover, West Africa is facing unprecedented population growth and most of them live in the country's capital. An increase of at least 105% is expected by 2050 which means that this region will face a drastic increase in industrial, domestic, and energy consumption. The stress on energy production will be exacerbated in the next coming years. Therefore, it is of paramount importance

to accurately forecast HWs in West African capitals in order to mitigate their socio-economic impacts.

Understanding HWs presents significant challenges since they are extreme events so infrequent and difficult to assess. The lack of suitable historical data for such extreme events, particularly in West Africa, further complicates their characterization. The challenge of constructing valid statistics for HWs is a significant obstacle in climate science, as gathering enough data to create accurate statistical models is numerically expensive and rare, making it difficult to assess model weather and climate biases for these extremes. This lack of understanding compromises the development of effective strategies to mitigate the effects of HWs on infrastructure and human health. However, the integration of Machine Learning (ML) with physical models offers a solution to address these challenges. By unlocking the potential of ML algorithms, it becomes possible to analyse large amounts of data and discover complex patterns in the mechanisms and life cycles of HWs. ML can also assist in detecting precursors and forecasting these events, which can help in developing early warning systems to mitigate their impact. Additionally, ML can help identify biases in climate models and improve their accuracy, leading to more accurate projections of future HWs (Jacques-Dumas et al., 2022). The complex nature of HWs and their infrequent occurrence highlights the need for innovative solutions to enable effective strategies for mitigating their impacts, and the integration of ML is one such solution.

2. Research questions

There have been fewer quantitative studies addressing the forecast of Heat waves in West Africa cities using model-based Machine Learning.

The main research question behind this study is:

How to enhance the short-term predictability of heat waves over Abidjan, the capital of Côte d'Ivoire using Machine Learning techniques?

The other questions behind the main one can be enumerated as followed:

- What is the temporal distribution of heat wave occurrences over Abidjan during the past years?
- Which Machine Learning-based model is most suitable for predicting heat waves based on meteorological conditions?

3.Research hypothesis

Heat waves occurrence will be more predictable through the complex understanding of Machine Learning-based models

- **The specific hypothesis:**

- Heatwave occurrences exhibit a specific temporal pattern.
- Heat waves forecasting over Abidjan using Artificial neural network (ANN) delivers good results.

4. Research objectives

Examine the predictability of heat waves over Abidjan city by using ML-based models.

- **The specific objectives:**

- Analyse the historical meteorological data to determine the temporal distribution and frequency of HW occurrences over Abidjan during the past years.
- Explore on the most suitable ANN architecture with relevant meteorological parameters as input for forecasting HWs over Abidjan

The following part of the document is organized into three distinct chapters, each contributing significantly to a comprehensive analysis of the subject. The chapter 1 conducts an extensive literature review, exploring various heatwave definitions used in scientific studies as well as the HI impacts, and challenges. Furthermore, it provides definitions and explanations of Artificial Intelligence (AI), ML, and DL. In chapter 2, attention is directed toward the materials and methods employed in this study. This section focuses on localizing the study area, elucidating the methodology for data collection, and explaining the chosen research approach. Moving forward, the chapter 3 presents the outcomes of the study and initiates a subsequent discussion. Finally, the remaing part encapsulates the overall findings, drawing insightful conclusions based on the results and discussing future research directions and perspectives to guide further investigations in the field.

CHAPTER 1: LITERATURE REVIEW

This section of the study begins with a review of the various definitions of HWs following by the potential repercussions of these catastrophic weather events on human health and livelihood. Furthermore, it provides specific definitions of AI, ML, and DL while emphasizing their interdependence. Moreover, the section also delves into a theoretical explanation of the Multi-Layer Perceptron (MLP), a fundamental component of the ANN group, clarifying its structural characteristics and learning mechanism.

1.1 Review of Heat wave definition

Investigating and debating a universally accepted definition of HW has been a subject of focus in the scientific community. However, quantitative definitions of HW differ in the heat measure used (Smith, Zaitchik, and Gohlke, 2013). Furthermore, most of the definitions employed in research highlighted various features, such as length, intensity, or suspended thresholds. Consequently, the lack of a uniform definition has resulted in disparities in the outcomes and findings of various investigations. The absence of a universally accepted scientific definition for a HW is attributed to its reliance on a wide range of factors, including the sector and region under examination. For instance, Smith, Zaitchik, and Gohlke (2013) assert that there is no singular, standardized definition for a HW. Moreover, experts hold differing opinions regarding the appropriate threshold values, duration, and supplementary variables to be included in HW definitions. Consequently, the comprehension of the frequency and magnitude of HW in each area or period is profoundly shaped by the HW definition chosen. In fact, varied definitions can lead to contrasting viewpoints regarding the occurrence and seriousness of such events. Supporting this, Tong, Wang, and Barnett (2010) agreed that even a minor adjustment in the definition of a HW had a significant influence on the anticipated health effects. Similarly, Barcena-Martin et al. (2019) reiterated that the reported frequency of HWs can be subject to change based on the chosen reference period and air temperature threshold in the definition. Notably, various definitions of HWs vary in their focus and inclusion of factors. In some cases, definitions exclusively focus on elevated temperatures that exceed a specific threshold for a designated period. In such cases, the emphasis is placed primarily on temperature levels. For example, Meehl and Tebaldi (2004), examine the impacts of HWs using two different definitions. The initial definition highlights the importance of the most severe heat

event happening every year. It also emphasizes the significance of consecutive nights with persistently high minimum temperatures during nighttime, as this has a significant impact on health. The second definition involves exceeding specific temperature thresholds, allowing for analysis of HW duration and frequency. Meehl and Tebaldi used the Parallel Climate Model (PCM) and the defined criteria to predict increased intensity, longer duration, and higher frequency of HWs.

In the study conducted by Pascal et al. (2013), a significant evaluation of the relationship between meteorological conditions and mortality outcomes was carried out. Meteorological indicators were established by calculating the average temperatures over three days, which involved taking the mean of the minimum and maximum temperatures for each day. To estimate the impact of these indicators on mortality, a Generalized Additive Model (GAM) was employed. The GAM considered factors such as long-term trends, seasonality, and day of the week. Thresholds were determined by analysing percentiles of Meteorological Indicator (MI) about excess mortality, specifically focusing on points of inflection in the excess mortality response. On another hand, (Fontaine, Janicot, and Monerie, 2013), in a study covering North Africa, employed observed and reanalysis data to investigate temperature changes, analyse HWs, and explore their relationship with atmospheric variables and circulation patterns. They examined the long-term evolution of temperature, hot days (HDs), and HWs, considering the mean seasonal cycle, and further inspected composite anomalies to identify specific changes independently.

In their study, HWs were defined by surpassing the 90th percentile of daily temperature variability, with a specific focus on durations of 4 days or longer to capture synoptic-scale events. (Russo et al., 2014) presented findings that highlighted the growing intensity of HWs worldwide. They introduced a metric called the Heat Wave Magnitude Index (HWMI), which includes both the intensity and duration of HWs by utilizing daily maximum temperatures and a threshold based on percentiles. The research encompassed three distinct periods and integrated climate model projections derived from the Coupled Model Intercomparison Project Phase 5 (CMIP5) across various Representative Concentration Pathways (RCPs).

Déqué et al. (2017) in another hand conducted a study in which they analysed 12 regional climate simulations from the COordinated Regional Downscaling EXperiment (CORDEX) ensemble for tropical Africa. They examined elevated temperatures to determine the occurrence of HWs. They

also defined a HW as a consecutive period of at least 3 days surpassing a temperature threshold, specifically set at the 90th percentile of the temperature distribution. Later, in a study conducted over the Sahel region, Barbier et al. (2018) used an approach that aims to identify and characterize HWs based on the intra-seasonal temperature fluctuations on multiple datasets for daily minimum and maximum temperature. To detect intra-seasonal temperature changes, they used a 90-day high-pass spectral filter to remove low-frequency components. Following that, the most significant temperature anomalies exceeding the 90th percentile for the period from March to July (1950-2010) were selected. Afterward, the most significant temperature anomalies exceeding the 90th percentile for the period from March to July (1950-2010) were selected. By doing so, they hoped to focus on HW episodes with a vast spatial extent, recording and evaluating larger-scale trends and their possible regional or global effects. In their case, (Batté et al., 2018) characterized HWs in West Africa as consecutive days when temperatures exceed the 90th percentile of the daily range of temperature of the region. They only deemed the seasonal variation in temperatures, particularly the elevated levels experienced during spring. To measure the occurrence of HWs, two indices are employed: the Heat Wave Duration Index (HWDI), which tracks the number of HW days per spring, and the Heat Waves per Period (HWPP), which counts the separate instances of heatwave events within the same season.

Lavaysse et al. (2018) on the other hand, defined HWs using a methodology that centers the transformation of daily minimum temperature and maximum temperature into quantiles, leveraging 21 years of climatological data. They divided each year into prolonged summer and winter periods to examine HWs and cold waves correspondingly. They then characterized HDs by both maximum temperature and minimum temperature surpassing the 90th quantile threshold, while cold days occur when temperatures for both variables dip below the 10th quantile threshold. HWs are characterized by a minimum of 3 consecutive HDs to account for the persistence of extreme temperatures and extreme waves. Heatwave duration and intensity are evaluated using three different calculation methods. Applying this methodology to the Sahel region reveals, an increase in the frequency and intensity of HWs, with a higher likelihood of occurrence during the extended summer period. Unlike the previous definitions, another group of scientists focused on the health aspect when defining HWs. Tong et al. (2015) investigated the possibility of developing a health risk-based definition for heatwaves and assessed the impact of heatwaves on mortality in

Brisbane, Melbourne, and Sydney three largest Australian cities. Furthermore, they defined HWs as periods of two or more consecutive days with daily mean temperatures above certain percentiles of the temperature distribution, where the relative risk of mortality starts to increase, sharpens, and rises alarmingly.

Xu et al. (2016) conducted a systematic review and meta-analysis in which various HW definitions used in the literature are examined. The study emphasizes the importance of HW intensity compared to duration in determining HW-related deaths.

Di Napoli, Pappenberger, and Cloke (2019) focus on proposing a health-based definition of HWs using the Universal Thermal Climate Index (UTCI). By examining UTCI values at different climatological percentiles, the research aims to identify correlations between specific UTCI thresholds and periods of excess mortality.

Conversely, Heo, Bell, and Lee (2019) in the same year, investigated the impact of HWs on health outcomes and compares different HW definitions. The study explored definitions based on thermal comfort and air temperature, particularly focusing on the Wet-Bulb Globe Temperature (WBGT) and its associated thresholds. By examining the relationship between HWs defined by WBGT and heat-related diseases, the research highlighted the potential of using WBGT as a reliable indicator to link HWs with adverse health effects.

Yu et al., (2021) conducted a study to examine the spatial-temporal variation of wet HWs over Eurasia from 1979 to 2017. Wet HWs were defined as periods lasting three or more days, where the Wet-Bulb temperature (WBT) exceeded the 90th percentile of the summer distribution. A study conducted by (Guigma, Todd, and Wang, 2020) in the Sahel region utilized a two-step process to detect HWs. They employed thermal indices including Temperature, Heat Index (HI), Steadman non-radiant Apparent Temperature (AT), Net Effective Temperature (NET), and UTCI. Initially, HDs were identified by calculating the 75th percentile of the thermal index data. Subsequently, the thermal index values were converted into anomaly values and filtered using a high-pass filter to retain variability. HWs were defined as consecutive sequences of at least three days that exceeded specific thresholds. Another recent study conducted by (Ngoungue Langue et al., 2022) focused on detecting HWs in West Africa. They used various indexes such as the daily minimum and maximum values of the two-meter air temperature, WBT, AT, and the UTCI. HWs were identified as consecutive days with extremely high indicator values surpassing a threshold. Three

methods are proposed: one for daytime HWs based on maximum indicator value, one for nighttime HWs based on minimum indicator value, and one for HWs occurring both during the day and at night. These methods use relative thresholds and consider the climatic conditions of the region. They allow for the monitoring and assessment of HWs associated with factors such as solar radiation and moisture content, thereby providing a better understanding of human health risks.

1.2 Impacts and challenges associated with heatwaves

The first consequence that comes to mind is the impact on human health. Indeed, HWs have been termed the silent killer (Loughnan, 2014) because their consequences on human health are not always immediate. It typically worsens pre-existing medical issues, primarily affecting the old, children, and those who labour outside, with death happening after several days. Because hospital admissions are frequently triggered by worsening sickness, precisely attributing mortality to heat extremes can be extremely challenging. As a result, the real number of heat-related deaths is likely to be underestimated (Perkins, 2015). Sherwood, Huber, and Emanuel (2010) state that increased exposure to heat stress could have major repercussions for human health in communities worldwide. Furthermore, in Africa, the effects of a maximum temperature of 2 degrees Celsius above the current climate could be disastrous for human health, given that monthly maximum temperatures already exceed 40 degrees Celsius in some areas. The capacity of the body to cool itself is put to the test in extreme heat and humidity situations. Exposure to high temperatures and humidity creates thermal professional stress that can have a significant impact on anyone working outside in hot environments or performing physical activities (Lucas et al., 2014; Takahashi et al., 2007). This may harm the productivity of people and health, having a negative influence on their well-being and, potentially, the national economy (Chen et al., 2017).

The West African region spans several climate zones with contrasting seasonal cycles (Diallo et al., 2014); it is densely populated and home to numerous transitional economies. As a result, it may be more vulnerable to changes in thermal stress. Therefore, the information on thermal stress predictions can thus assist decision-makers in developing strategies for the most vulnerable areas to protect worker health and productivity through mitigation or adaptation measures. During the early 21st-century HWs, animals in both terrestrial and marine environments died in greater numbers. Summer HWs cause animal population death, making it a season of stress and survival,

affecting populations and ecosystems. Although HWs are only present for a brief length of time in an animal's life, they only need to occur once during the pre-reproductive development period to significantly affect reproductive success (Stillman, 2019).

1.3 Artificial intelligence, Machine Learning, and Deep Learning

The field of AI has garnered significant attention and active discussion within the scientific community. Extensive studies have been conducted to explore the theoretical aspects of AI technologies and their practical applications across various domains of our society. AI, ML, and DL have particularly attracted heightened interest in recent years. This growing interest is reflected in the increasing number of publications found in scientific databases. Figure 1 demonstrates the expanding research efforts in this field.

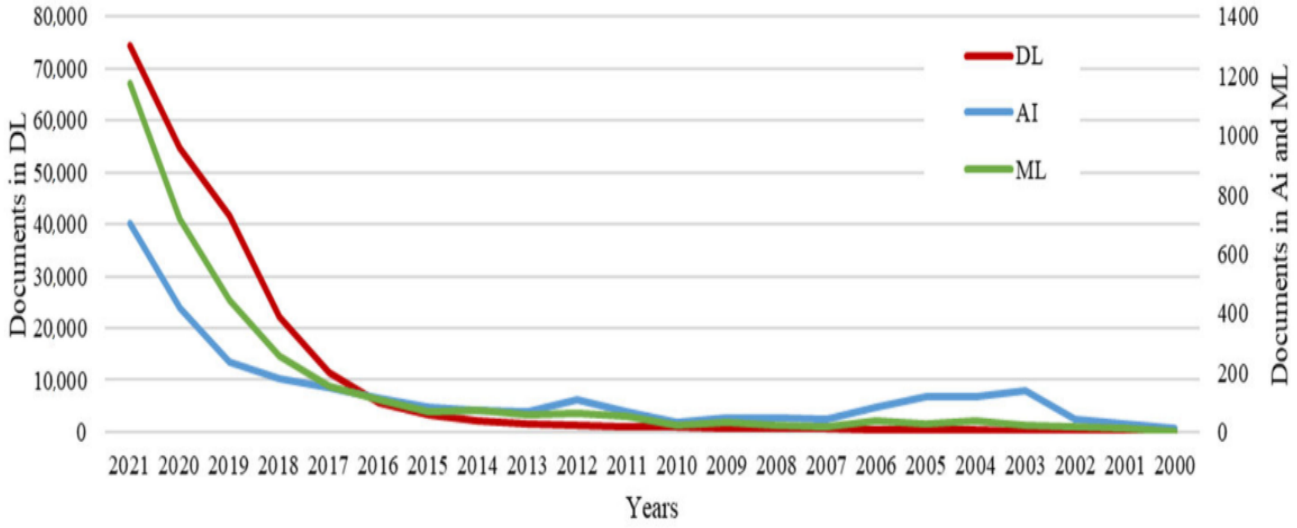

(Mukhamediev et al., 2022)

Figure 1: Evolution of AI in scientific research

1.4 Artificial intelligence

AI, a subfield of applied computer science, has grown at an exponential rate and has been integrated into a wide range of fields. The adoption of modern technology to better human lives has resulted in the development of outstanding AI applications. Apple's Siri, Amazon's Alexa, Hanson Robotics' Sophia, IBM's Watson machine, and Tesla's driverless automobiles are all examples. Human-computer interaction, machine-machine communication, and the incorporation

of intelligence into devices and objects have all enabled the incorporation of intelligence into machines. As a result, machines such as Sophia, a humanoid robot, have begun to exhibit human-like behavior. AI is a multidisciplinary discipline that includes computer science, electronics, communication, engineering, basic sciences, and even the humanities and social sciences. Its applications range from household science to environmental studies, linguistics to history, and more. Machines can perform cognitive processes similar to human capabilities using AI, such as perception, reasoning, learning, and interaction. Although AI has faced limitations such as restricted research and development, processing power, and data availability, the demand for automation of human situations has accelerated its growing commercial presence today.

1.5 Machine learning

ML is an area of AI that allows machines to learn from data and improve their prediction accuracy without requiring human intervention. In other words, it allows machines to learn on their own by following a set of instructions. The primary idea behind ML is to mimic how the human brain works. ML is frequently used to characterize developments in systems that perform AI-related tasks (Rasmussen & Williams, 2006).

Apart from self and rote learnings of traditional learning modus operand, other learnings such as supervised, unsupervised, semi-supervised, reinforcement, DL, and TL come under the umbrella of ML. Let's briefly pass through these enumerated concepts.

- **Supervised Learning:** Supervised Learning (SL), a type of ML, is a technique in which machines learn from algorithms that have been programmed and labelled data. It involves providing the machine's input data and accompanying labels. The supplied data comprises model development features. Computers learn with guided instructions from algorithms in Supervised ML. The output can be in the form of instructions, formulas, algorithms, or diagrams. These models are critical for real-time data validation in a variety of applications (Madakam et al., 2022).
- **Unsupervised Learning:** The second type of ML is unsupervised learning, which involves self-learning without explicit training. It is a time-consuming and sophisticated procedure that relies on computer device input data and built-in algorithms. Unlike supervised learning, unsupervised learning not require labelled output data. Instead, It focuses on

exploratory data analysis and detecting hidden patterns or data grouping. Wang (2016) emphasized its capacity to categorize data without explicit training. Programmers support a seamless procedure to attain the desired output in unsupervised learning by utilizing pre-developed algorithms.

- **Reinforcement Learning:** Another variant of ML is reinforcement learning, which focuses on how software agents should behave in a virtual environment to optimize the concept of cumulative reward. In other words, reinforcement learning is a learning paradigm that aims to educate a system how to regulate itself in order to maximize a numerical performance measure that communicates a long-term goal (Madakam et al., 2022). Instead of accurately labelled instances, as is typically the case in other ML scenarios, the reinforcement learning paradigm is a popular technique for handling issues with little environmental feedback (Taylor and Stone, 2009). Reinforcement learning provides a framework and a collection of tools for building complex and difficult-to-design behaviours in robots (Kober, Bagnell, and Peters, 2013).

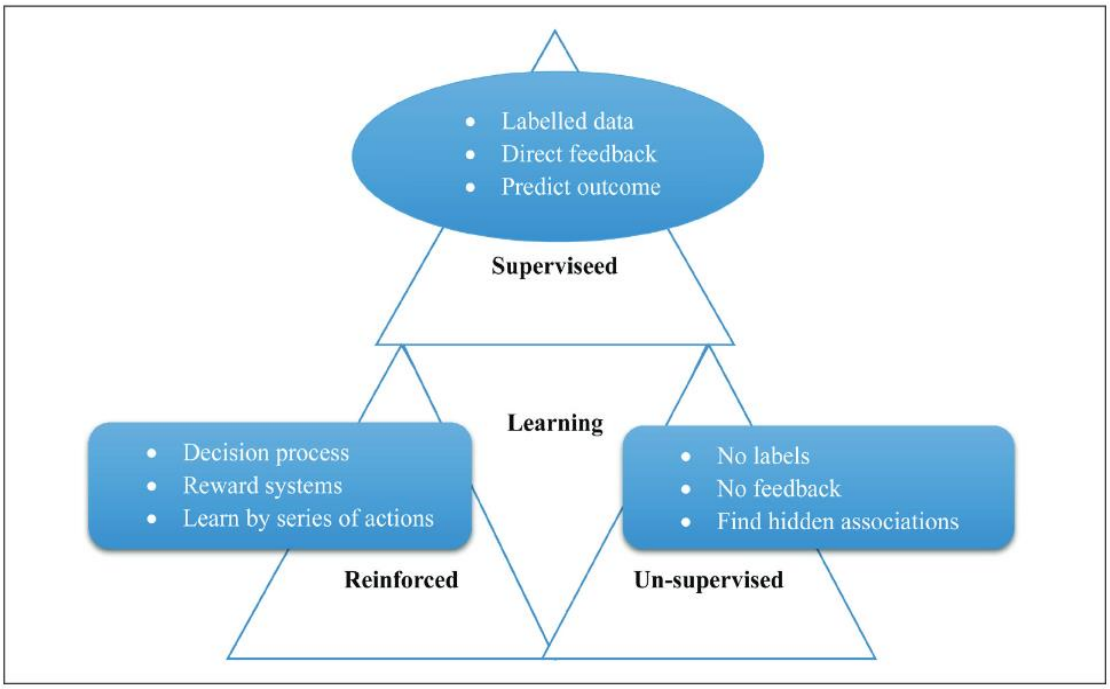

(Madakam et al., 2022)

Figure 2: Machine Learning Categories

- **Deep Learning:** DL is a set of methods that employ the so-called deep neural networks (DNNs), in other words, the networks containing two or more hidden layers. The main advantage of deep architectures is related to the ability to solve tasks using the end-to-end method. This approach reduces the requirements for preliminary data processing since a signal or image vector is used as an input to the network, and the network independently identifies the regularities relating the input vector to the target variable. The network selects the significant characteristic, which is a time-consuming and complex procedure (Mukhamediev et al., 2022).
- **Transfer learning:** TL has emerged as a new paradigm shift in DL, gaining popularity for its ability to train DNN with limited data (Zhu et al., 2011). By leveraging auxiliary source data from related domains, TL enables the utilization of previously acquired knowledge to solve new but similar problems, resulting in significant time and resource savings while reducing costs (Lu et al., 2015). Torrey and Shavlik (2010) define TL as the improvement of learning in a new task through the transfer of knowledge from a related task that has already been learned. Additionally, TL addresses the challenge of effectively utilizing labelled data from a source domain to tackle different problems in a target domain, even when the distributions or features of the training and testing data differ (Fachantidis et al., 2013; Pan et al., 2008).

1.6 Artificial neural networks: theory

ANN is a supervised learning strategy in DL that is an approximation of the biological neural network in the human brain (Do Carmo Nicoletti & Jain, 2009). It is composed of three layers: input, hidden, and output, and each layer contains an array of artificial neurons (perceptron). A completely connected neural network is one in which every neuron in any given layer is connected to every neuron in the next or previous layer. An artificial neuron is a mathematical model with components that are similar to those of a real neuron (Figure 3). The input layer stores the array of input parameters, and each input variable is represented by a neuron. Each of these inputs is changed by a weight (also known as a synaptic weight) whose function is akin to that of a synaptic junction of a biological neuron.

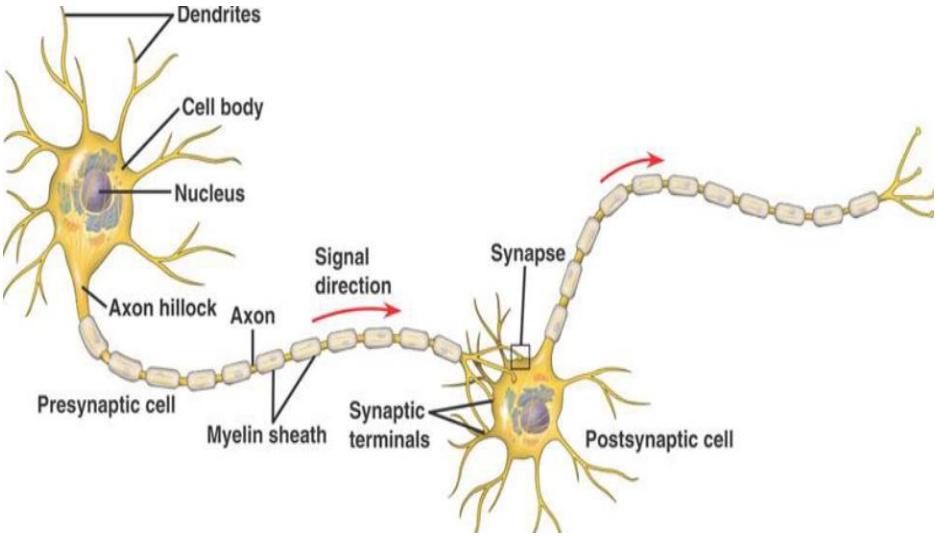

(HITZIGER, 2015)

Figure 3: The simple structural map of a biological neuron

1.6.1 Perceptron

The perceptron is one of the fundamental building blocks of ANNs. Invented by Franck Rosenblatt, (1957), it is a type of binary classifier that takes in multiple input values and produces a single output value that is either equal to 0 or 1. Figure 4 illustrates the workflow of a perceptron with two input values (X_1, X_2), each with its weights (W_1, W_2) and a bias (b) with a rule to adjust the boundary.

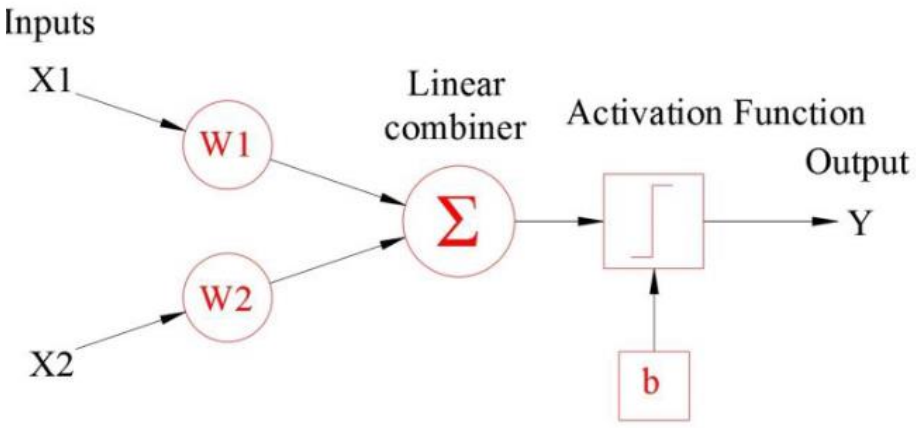

(HITZIGER, 2015)

Figure 4: The algorithm of a synthetic neuron that mimics a human neuron

The process of this perceptron can be described using the following set of equations:

$$Z = (W_1 \ W_2)\begin{pmatrix} X_1 \\ X_2 \end{pmatrix} + b \qquad \text{(Eq 1)}$$

$$Z = W_1 \cdot X_1 + W_2 \cdot X_2 + b \qquad \text{(Eq 2)}$$

Z is the linear aggregation of the input values and their corresponding weights

$$Y = f(Z) \qquad \text{(Eq 3)}$$

Y is the activation function, which introduces non-linearity into the decision-making process of the perceptron. The possible value of Y are either 0 or 1, depending on the value of Z

$$Y = \begin{cases} 1, & \text{if } Z > 0 \\ 0, & \text{otherwise} \end{cases} \qquad \text{(Eq 4)}$$

In the case of a general perceptron, with multiple input (X_1, X_2, …, X_n), the equation (Eq 4) becomes:

$$Y = \begin{cases} 1, & \text{if } \sum_i W_i X_i \\ 0, & \text{otherwise} \end{cases} \qquad \text{(Eq 5)}$$

The perceptron starts off with randomly initialized weights for the initial stage of the training process. These weights are the starting points for the learning algorithm of the perceptron, which seeks to optimize them to get the desired output, this algorithm is called the gradient descent.

$$\epsilon = Y_{true} - Y_i \quad \text{(Eq 6)}$$

$$\acute{W}_i = W_i - \alpha \cdot \epsilon \cdot X_i \quad \text{(Eq 7)}$$

ϵ : The error calculation for the current input sample Xi.

α : The learning rate is a hyperparameter that regulates the step size or amplitude of weight. Changes during training. It controls how fast or slow the model learns from training data.

$\acute{W}_i$: The updated parameter.

The purpose of the perceptron is to minimize classification error by adjusting the weights and bias. This fundamental premise is shared by all ANNs (Staudemeyer & Morris, 2019).

1.6.2 Perceptron constraint

When shown graphically, the aggregation function of a perceptron creates a straight line that depends on the values W_1, W_2, and b. Because of this linearity, the perceptron can divide data into two classes based on a decision boundary. As a result, when confronted with a nonlinear situation, this approach has limitations (Figure 5).

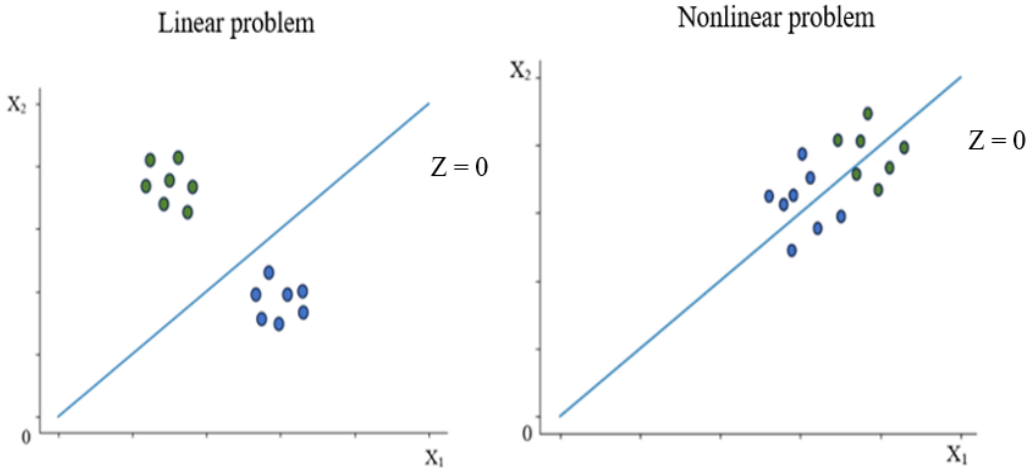

Figure 5: Illustration of the limitation of a perceptron for a nonlinear problem

1.6.3 Multi-Layer Perceptron

The MLP architecture is a feedforward neural network (Figure 6), which is one of the most basic and extensively used neural network architectures. It is made up of three kinds of layers: the input layer, the hidden layer(s), and the output layer.

Input Layer: The input layer is the initial layer in the MLP architecture and serves as the data entering point. Each neuron (perceptron) in the input layer represents a different aspect or feature of the input data. The number of neurons in the input layer depend on the dimension of the input data.

Hidden Layer(s): The hidden layer(s) are layers that sit between the input and output layers. Their neurons are called hidden because they are not directly exposed. Depending on the complexity of the problem and the required network capacity, the number of hidden layers and neurons in each hidden layer can be altered. Each neuron in the hidden layer(s) gets input from all neurons in the preceding layer (either the input layer or the preceding hidden layer) and applies a mathematical adjustment to these inputs.

Output Layer: The output layer is the last layer in the MLP design and is responsible for producing the predictions of the network. The nature of the task determines the number of neurons in the output layer. In a binary classification problem, for example, the output layer will typically consist of one neuron representing the likelihood of belonging to one class. The output layer in a multi-class classification issue will include several neurons, each reflecting the likelihood of belonging to a certain class. The output layer in regression tasks consists of a single neuron that predicts a continuous value.

The connections between neurons in the MLP are usually fully linked, which means that each neuron in one layer is connected to every neuron in the next layer. Each link has a weight that determines the strength or relevance of the connection. These weights are learned during the training phase to improve the performance of the network.

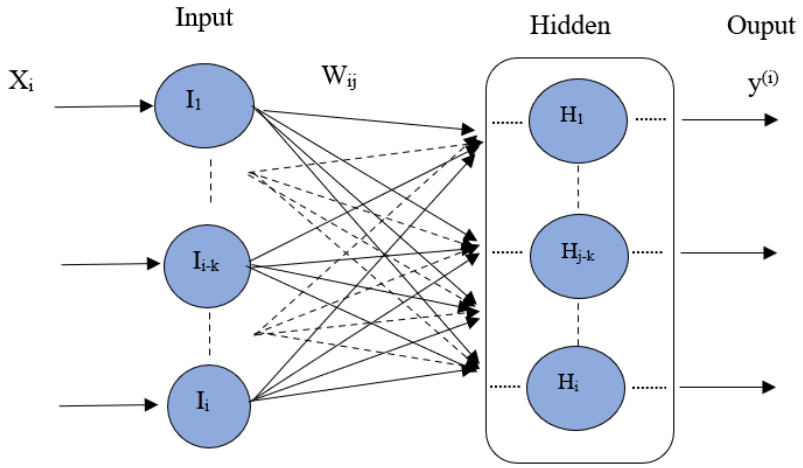

Figure 6: Artificial neural network architechture

X_i : Input data

W_{ij}: Weights of the ANN

I_i and H_j: The neurons in the input and hidden layers, respectively

$y^{(i)}$: The output of the model

1.6.4 Activation functions and their role in MLP

Activation functions play a crucial role in MLP and ANN architectures in general by introducing non-linearity into the network. They are applied to the outputs of individual neurons in the hidden layers and the output layer of the network. The choice of activation function affects the network's ability to learn complex patterns and make accurate predictions (Kiliçarslan et al., 2021; Rasamoelina et al., 2020).

Some commonly used activation functions are:

Sigmoid (σ) Function: The sigmoid function, also known as the logistic function, takes a real-valued input and maps it to a range between 0 and 1. The sigmoid function is useful in MLPs for binary classification problems where the output represents the probability of belonging to a certain class, and it can also be used in the hidden layers.

Rectified Linear Unit (ReLU): ReLU is a popular activation function in DL. It returns the input as the output if it is positive, and 0 otherwise. ReLU is computationally efficient and helps the network learn faster during training.

Hyperbolic Tangent (Tanh) Function: The hyperbolic tangent function is similar to the sigmoid function, but maps the input to a range between -1 and 1. Like the sigmoid function, the tanh function is useful for binary classification and can be used in hidden layers.

The sigmoid activation function : $\sigma(x) = \frac{1}{1+ e^{-x}}$ (Eq 8)

The ReLU activation function : $\mathrm{ReLU}(x) = \max(0, x)$ (Eq 9)

The Hyperbolic tangent activation function : $\mathrm{Tanh}(x) = \frac{e^{x}-e^{-x}}{e^{x}+e^{-x}}$ (Eq 10)

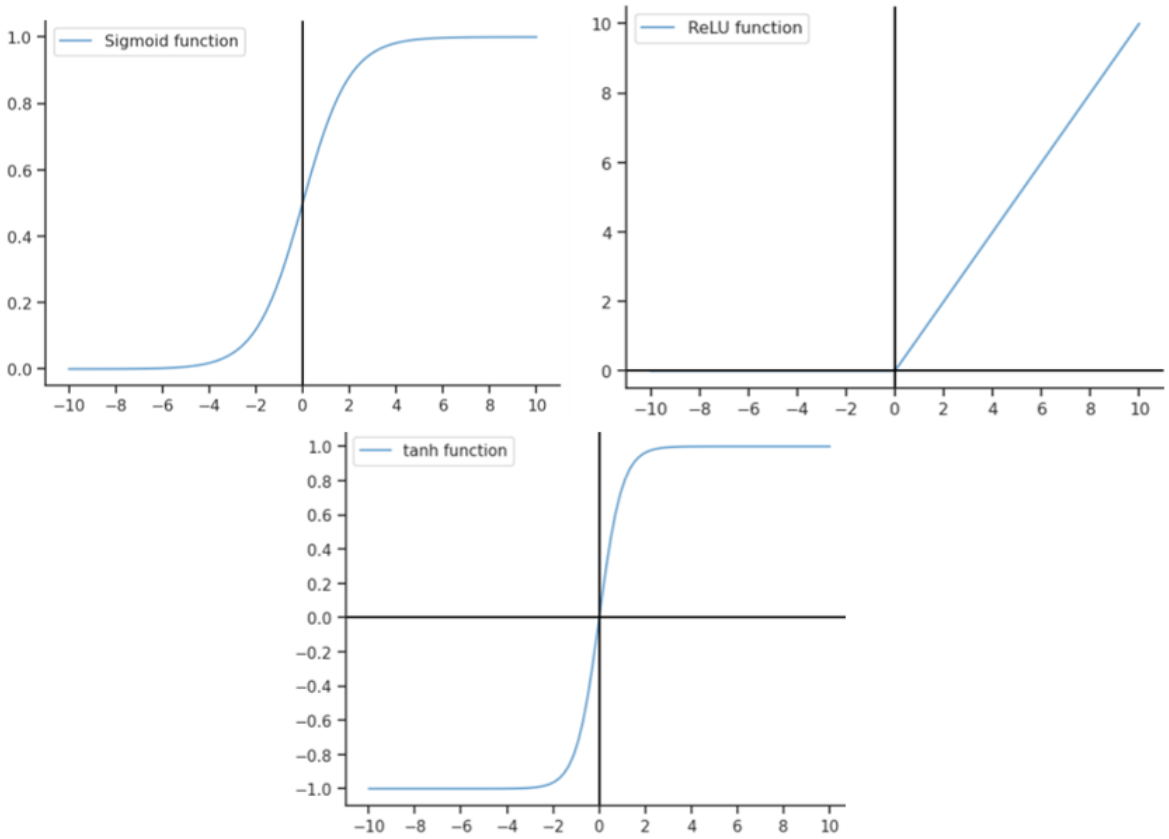

Figure 7: Sigmoid, ReLU and tanh activation functions.

1.6.5 Theory of the backpropagation technique in MLP training

The backpropagation algorithm is a fundamental technique used to train MLP neural networks. It is an efficient way to compute the gradients of the specific loss function with respect to the

network's weights. By iteratively adjusting the weights based on these gradients, the backpropagation algorithm enables the network to learn and improve its performance over time.

The main steps involve are:

Forward Propagation: During forward propagation, the input data is fed through the network, and the output is computed. Each neuron in the network receives inputs from the previous layer, applies a weighted sum operation, and passes the result through an activation function. This process is repeated layer by layer until the output is obtained.

Loss Calculation: After obtaining the network's output, the difference between the predicted output and the true output (target value) is computed using a loss function. Common loss functions include mean squared error (MSE) for regression problems and cross-entropy for classification problems.

Backward Propagation: The main step of the backpropagation algorithm is to propagate the error gradient backwards through the network. Starting from the output layer, the algorithm calculates the gradient of the loss function with respect to the weights and biases of each neuron in the network.

Weight Update: Once the gradients have been computed, the weights and biases are updated to minimize the loss function. This is typically done using an optimization algorithm like gradient descent or one of its variants. The weights are adjusted in the opposite direction of the gradient, scaled by a learning rate that controls the step size of the updates.

1.7 Case Studies and Research on Heatwave Prediction Using AI and ML

ML has greatly improved the interpretation and performance of General Circulation Models (GCMs). As proven by Kurth et al. (2018) and (Lagerquist et al., 2019) studies, DNNs in particular have been successfully employed to identify extreme weather and climate trends in both actual and modeled atmospheric states. Furthermore, as demontrated by Herman & Schumacher, (2018), ML algorithms are effective in predicting extreme weather events. For example, in a study where a random forest model was developed by (Park et al., 2020) for weekly heat damage prediction based on four years (2015-2018) of statistical, meteorological, and floating population data in South Korea. According to the results, the suggested model surpasses existing models. Shi et al.

(2021) in an article present a method for investigating the spatial heterogeneity of HW conditions using ML and geospatial mapping approaches. Indeed, they used a spacial buffer analysis and random forest ML technique to identify important influential HW variables, providing valuable information for appropriate urban planning to improve resilience against HW events and heat-related disasters. Using open urban data, their approach directly maps the spatial distribution of HW conditions, incorporating spatial variability into HW estimation. Jacques-Dumas et al. (2022) used DL techniques to forecast future instances of long-lasting intense HWs in a study concentrating on the application of ML technology to analyse unusual HWs and evaluate their prediction. The researchers used data from 1000 years of climate models to develop an algorithm capable of forecasting HW occurrences using surface temperature and geopotential height data.

1.8 Host institut

Acronym: SODEXAM

Institute Name: Société d'Exploitation et de Développement Aéroportuaire, Aéronautique et Météorologique

Official Website: https://www.sodexam.com/

Established: 1997

Location: Abidjan, Côte d'Ivoire

Areas of expertise: Air navigation, airfields, airport security and facilitation, aviation and airport medicine, meteorology, and other related sectors.

Mandate: The management, operation, and development of airports, meteorology, and aeronautical activities in Côte d'Ivoire.

Main missions:

- Management of air traffic control, fire safety, aeronautical meteorology, and aeronautical telecommunications services at Ivorian airports open to public air traffic.
- Management of airport, aeronautical, and meteorological infrastructures on behalf of the State.
- Management of the commercial facilities and movement areas at Ivorian airports open to public air traffic, excluding licensed airports.
- Conduction and coordination of observation, study, and forecasting activities in meteorology and specialized sectors.
- Undertake the implementation and oversight of aeronautical, airport, and meteorological investments and projects funded by the State, utilizing its available resources and under the supervision of governing ministers.
- Management of ground handling activities at airports, subject to existing agreements. They also monitor and control airport concessions and establish master plans for airports open to public air traffic.
- Coordination of the activities of all public and private services related to airport operations.
- Representation of the State in its field of competence and maintains relations with international organizations involved in aviation and meteorology.
- Engagement in industrial, commercial, securities, real estate, and financial operations that contribute to the development of airports and meteorological stations within the country, directly or indirectly related to its activities.

In conclusion, this literature review section has emphasized the persistent challenge associated with defining HWs and the significant impact of this infrequent yet extreme climatic phenomenon on human well-being and livelihood. Moreover, the scarcity of studies employing AI-based models to address HWs has been identified as a notable gap in the existing research landscape. To bridge this gap, the present study aims to employ the MLP and TL techniques as innovative approaches to predict this rare meteorological event. By leveraging these computational methods, this research endeavours to contribute to the development of accurate and effective predictive models for HWs, ultimately aiding in the mitigation of their adverse consequences on human health and societal systems.

Chapter 2: Material and Method

The present section attempts to provide detailed insights into the area of study, the research tools used, and the methodology used to effectively answer the objectives of this research.

2.1 Study area

Firstly, the present section will present the location of the study area, elucidating its geographical coordinates, topographical features, and surrounding environment. Secondly, the section will delve into a detailed description of the climate within, encompassing factors such as temperature patterns, precipitation levels, and vegetation characteristics. By examining these crucial elements, the study aims to establish a robust understanding of the environmental dynamics within the specified region.

2.1.1 Location

Located in the south-eastern part of Côte d'Ivoire between Latitudes 5°10 and 5°38 North and Longitudes 3°45 and 4°21 West in geographic coordinate system (WGS 84, zone 30 N) (KOUAKOU, 2020), Abidjan, the capital of Côte d'Ivoire, is the most populated city in French-speaking West Africa, accounting for 20% of the entire population of the country of around 6,351,086 people. Located between this bustling economic capital covers an area of 422 km^2, resulting in a population density of roughly, 15050 people per square kilometre. Abidjan's urban landscape is diversified and active, with over 280 separate neighbourhoods. The city of Abidjan is separated into two sections: Abidjan North and Abidjan South. Plateau, Adjamé, Attécoubé, Cocody, Yopougon, and Abobo are in the northern region, while Treichville, Marcory, Koumassi, and Port-Bout are in the southern region. The gorgeous Ebrié Lagoon separates these two sections, with Abidjan North representing the city's mainland and Abidjan South encompassing the territory between the lagoon and the sea. Abidjan is located in a climatic zone that extends from the 8^{th} parallel to the coast and covers the lower part of Côte d'Ivoire. The city has a sub-equatorial climate with four distinct seasonal episodes, including two rainy seasons and two dry seasons. This meteorological pattern, along with considerable human activity, adds to the city's lack of significant greenery (Sylvain Gnamien, 2022; Ymba, 2022).

2.1.2 Climate

Abidjan has an equatorial-sub-equatorial transition climate (Attieen Climate). This climate has four distinct seasons that occur throughout the year: a long dry season from December to May, followed by a long wet season from May to July. Following that, there is a brief dry season from August to September, followed by a brief wet season from October to November (Tapsoba, 1995). The total annual rainfall ranges from 1718.38 mm to 1169.42 mm (1982-2018), with higher maxima at 29.54 ° C and lower minimum at 23.84 ° C. Throughout the year, the region experiences stable thermal patterns and is impacted by a southwest monsoon breeze. Temperatures stay largely steady regardless of whether the month has substantial rainfall or less rainfall (Ahoussi et al., 2013; KOUAKOU, 2020).

- Temperature

According to the data, the minimum temperature follows a wave throughout the year, with maximums in March and April (on average of 25.84 °C for April) and the coolest month in August (on average of 22.66 °C). Maximum temperatures follow the trend of minimum temperatures, with maximums in February (29.54 °C, warmer months) and minimums in August (26.48 °C). The mean temperature follows the same trend as the maximum temperature, with the maximum in the same month (27.64 °C) and the minimum in August (24.22 °C), so February and August are the extreme months for temperature (27.64 °C-24.22 °C) (KOUAKOU, 2020).

- Precipitation

The rainfall pattern has two modes. The average monthly rainfall varies greatly throughout the year. The long rainy season lasts from May to July, with a peak of 269 mm in June, whereas the short rainy season lasts from October to November, with a peak of 142.8 mm in October. The average yearly precipitation during the previous 36 years (1982-2018) has been 1410.07 mm/year. The long dry season lasts from December to April, and the short dry season lasts from August to September (KOUAKOU, 2020; Kouassi, 2021).

- Vegetation

Turraeanthus Africanus, which thrived in relatively nutrient-deficient clayey soils, was the main flora in the Abidjan region. This forest, however, was destroyed to enable the expansion of Abidjan city and to facilitate agricultural activity. The Banco National Park currently contains only a little remnant of the forest. The pre-lagoon savannas have distinct ecological characteristics due to their location on sandy soils generated from the Continental Terminal (Tastet, 1979). Mangrove forests and saline hydromorphic alluvial soils are both small. They are located on the flat shores of estuaries and lagoons, and their wood and bark are highly valued (BNETD, 2008). Swamp woods dominate the coastal stretch.

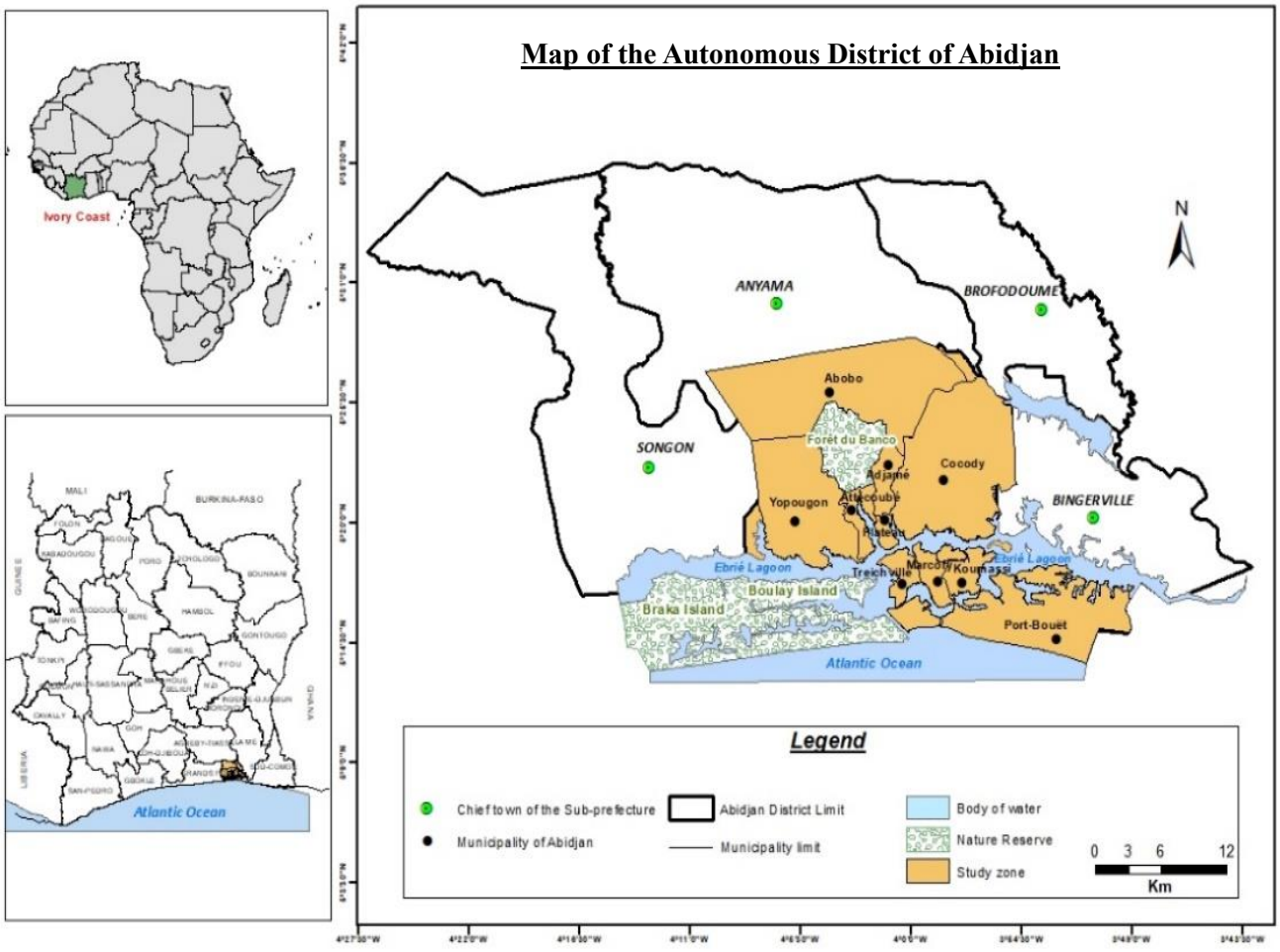

Figure 8: Study area

2.2 Data collection

Two ensembles of data have been used in order to achieve the aim of this study. The first dataset used for this work is the ERA5-Land, available on the Copernicus website. ERA5-Land is a reanalysis dataset that provides a more comprehensive and expanded perspective of land variable evolution over multiple decades than ERA5 (Muñoz-Sabater et al., 2021). The ERA5-Land dataset have been downloaded in the netCDf format with a horizontal resolution of 0.1° x 0.1°, which translates to a native resolution of approximately 9 km. In terms of vertical coverage, ERA5-Land spans from 2 meters above the surface level down to a soil depth of 289 cm. The variables

concerned by our study are the 2-meter temperature, the 2-meter dew point temperature and the surface pressure. This dataset also covers the period from 1961 to 2022, either 61 years of data.

The second dataset used in this work is a three hourly historical observation data collected from the synoptic station in Abidjan. The dataset covers the period from 2009 to 2022 which is equivalent to 13 years of data. The variables are also the same with those inside the ERA5 data.

2.2.1 Justification of the variables

Temperature: Temperature is a key characteristic that is directly related to HWs. HWs are defined by protracted periods of extremely high temperatures. The magnitude and intensity of HW episodes can be captured by introducing temperature as a variable. Tracking temperature changes over time can provide useful information about the occurrence of HWs (Jacques-Dumas et al., 2022; Meehl & Tebaldi, 2004; Pascal et al., 2013).

The dewpoint temperature: The dewpoint temperature is the temperature at which air becomes saturated with water vapor, resulting in condensation and, potentially, cloud or precipitation development. This measure aids in determining the moisture content of the air. HWs can include not just high temperatures, but also high humidity levels, which can aggravate the discomfort and health hazards connected with HWs (Lucas et al., 2014). The availability of this component in the dataset gives humidity information, which appears to be a crucial characteristic to consider when determining the consequences of HWs on health.

The atmospheric pressure: The atmospheric pressure exerted at the Earth's surface is referred to as surface pressure. It has a significant impact on weather patterns and can influence the genesis and duration of HWs (Hirsch et al., 2019). Variations in surface pressure can have an impact on the movement of air masses, the creation of high-pressure systems associated with HWs, and the atmospheric stability. The addition of surface pressure as a variable provides for a more complete understanding of the meteorological circumstances that contribute to HW episodes.

2.3 Tools

The main programming language utilized throughout the entirety of this work is Python. Python was chosen as the primary language because of its versatility, wide library support, and syntax simplicity. Python implementation has been made possible by the use of two major platforms: Spyder from the Anaconda environment and Google Colab.

The Anaconda environment, specifically the Spyder Integrated Development Environment (IDE), was critical all along this work. Anaconda is a comprehensive platform for scientific computing and data analysis, with numerous libraries and tools pre-installed. Spyder, in particular, has aided in the processing and interpretation of climate data by allowing for rapid data editing, visualization, and statistical computations. Its user-friendly interface and sophisticated capabilities have substantially expedited the research's data processing phase.

In addition to the Anaconda environment, Google Colab was useful in the creation of the DL model. Google Colab, a cloud-based Jupyter Notebook environment, integrates seamlessly with other Google services and provides access to computational resources such as GPUs and TPUs. The DL models were effectively trained and assessed using the power of Colab

The libraries used all along the work are:

Pandas: An open-source data analysis and manipulation tool that is fast, powerful, flexible, and simple to use. It was used in the management of data structures.

Numpy: A fundamental Python library for scientific computing. It has been used for the management of multidimensional arrays.

Xarray: A Python library for manipulating labelled multidimensional arrays. It was used to manage the netCDF files.

Metpy: A Python library that contains utilities for reading, displaying, and calculating weather data. It has been used to compute weather parameters.

Matplotlib and Seaborn: Versatile libraries allowing effective produce static, animated, and interactive visualizations. They have both been for data visualization.

Keras: An open-source DL framework written in Python. It has been used for building training validation and validating the DL model.

KerasTuner: A scalable, user-friendly hyperparameter optimization system. It has been used to ease the difficulties associated with hyperparameter search.

Scikit-learn: A simple and efficient tool for predictive data analysis built upon SciPy. It has mostly been used for model evaluation.

2.4 Method

The section will firstly delve into the specific definition employed for characterizing HWs in Abidjan. Subsequently, an in-depth explanation of the model implementation will be provided, elucidating the technical details and methodologies employed. Lastly, the evaluation metrics utilized to assess the performance and accuracy of the model will be detailed.

2.4.1 Heat index

Before delving into the subject of HWs, let us first explore the index used to characterize them. The HI parameter has been used in some research to investigate HWs (Guigma et al., 2020; Rome et al., 2019). Developed by R. G. STEADMAN (1979), the HI determines an apparent temperature by combining air temperature and relative humidity (RH). Indeed, the evaporation rate of water is lowered when the RH is high. This means that heat is evacuated from the body at a slower rate, allowing it to retain more heat than in dry air (McGregor et al., 2015).

The following formula was used to calculate the HI:

$$HI = C_1 + C_2 \times T + C_3 \times RH + C_4 \times T \times RH + C_5 \times T^2 + C_6 \times RH^2 + C_7 \times T^2 \times RH + C_8 \times T \times RH^2 + C_9 \times T^2 \times RH^2 \quad \text{(Eq 11)}$$

(R. G. STEADMAN, 1979)

C_1 = -42. 379, C_2 = 2,04901523, C_3 = 10,14333127, C_4= − 0,22475541, C_5 = $-6{,}83783 \times 10^{-3}$, C_6= $-5{,}481717 \times 10^{-2}$, C_7= $1{,}22874 \times 10^{-3}$, C_8 = $8{,}5282 \times 10^{-4}$, C_9 = $-1{,}99 \times 10^{-6}$

HI (in degrees Fahrenheit), T (ambient temperature in Fahrenheit), RH (relative humidity from 0 to 100%)

2.4.2 Heat wave definition

As pointed out in Chapter 1, precisely quantifying HW is quite challenging. Various definitions of HW exist depending on the context and area of study. The methodology used to determine HW in this study is based on the study conducted by Rome et al. (2019). Given the ongoing trend of global warming, it is important to either raise the absolute threshold or use a relative threshold. Accordingly, HW refers to a situation in which the daily maximum HI reachs or surpasses the 90th percentile value of its distribution for at least three consecutive days.

Based on the dataset, the establishment of the HW detection threshold has been done differently.

Era5 data case: A subset of ERA5 data was extracted from a grid point near the Abidjan synoptic station using nearest neighbour interpolation, ensuring that the analysis captures the localized weather conditions in that area. By narrowing down the analysis to the data near the synoptic station, it focuses on the relevant information for that specific location. This subset contains observations geographically close to the synoptic station, ensuring the analysis captures the localized weather conditions in that area.

The ERA5 data was divided into two parts, spanning the periods of 1961 to 1990 and 1991 to 2022, respectively. The initial step involved applying the 90th percentile to the daily maximum HI values from 1961 to 1990. Subsequently, the same 90th percentile value derived from the earlier period (1961 to 1990) was utilized to identify HDs within the daily maximum HI data from 1991 to 2022.

Abidjan synoptic station data case: The calculation of the HD's threshold involved utilizing the available data period, which extended from 2009 to 2022. The threshold for detecting HDs using the Abidjan synoptic data was determined based on the obtained value as the 90th percentile of the daily maximum HI.

2.4.3 Heat wave prediction dataset

In the context of supervised learning, the acquisition of a pertinent dataset is imperative for a model to acquire the necessary knowledge and generalize it toward accurate predictions on novel instances. In our case study, The model takes as input the daily average specific humidity, average potential temperature, and maximum WBT.

The computation of these variables have been possible using the MetPy package following the formulas below:

- Potential temperature

$$\theta = T \times \left(\frac{P_0}{P}\right)^k \quad \text{(Eq 12)}$$

P_0 = 1000hPa,

$k = R/c_p$

c_p = 1005 J/(kg·K) the specific heat capacity at constant pressure of the dry air

R = 287 J/(kg·K) the gas constant.

T: the temperature in kelvin (K)

- Specific humidity

$$q = \frac{0.622 \times e}{P - e} \quad \text{(Eq 13)}$$

With q the specific humidity and p the surface pressure

With (e) the saturation vapour pressure which is computed from the following formula:

$$e = 6.1094 \times e^{\left(\frac{17.625 \times T}{T + 243.04}\right)} \quad \text{(Eq 14)}$$

(Tetens, 1930)

- Wet bulb temperature

$$T_w = T \times \operatorname{atan}\left[0.151977 \times (RH + 8.313659)^{\frac{1}{2}}\right] + \operatorname{atan}(T + RH) - \operatorname{atan}(RH - 1.676331) + 0.00391838 \times (RH)^{\frac{3}{2}} \times \operatorname{atan}(0.023101 \times RH) - 46860335 \quad \text{(Eq 15)}$$

(Stull, 2011)

These parameters were chosen for their inherent relationship with both humidity and pressure rather than for the variables in the dataset.

It is essential to underscore that rather than predicting the complete temporal extent of a HW, the methodology prioritizes the identification of individual days that are likely to be hot.

2.4.4 Methodology to implement the model

To accomplish the objectives of this study, two distinct models have been constructed utilizing separate methodologies and dataset. Firstly, an optimized Multiple Linear Perceptron (MLP) model was meticulously trained on a comprehensive dataset spanning 31 years of daily ERA5 data. Subsequently, the acquired knowledge and capabilities of the pre-trained model were leveraged by the final MLP model to discern intricate patterns within synoptic data. This approach was undertaken to address the challenge associated with the infrequent incidence of HD events in the synoptic data specific to Abidjan city.

The figures below presents a brief overview of the methodology used to implement the MLP models. The text in blue represent the package used for the specific step of the methodology, and those in orange represent the main methods used during this step.

The core elements of the process will be covered in detail in the next subsections, which will also ensure its reproducibility by meticulously presenting all necessary information.

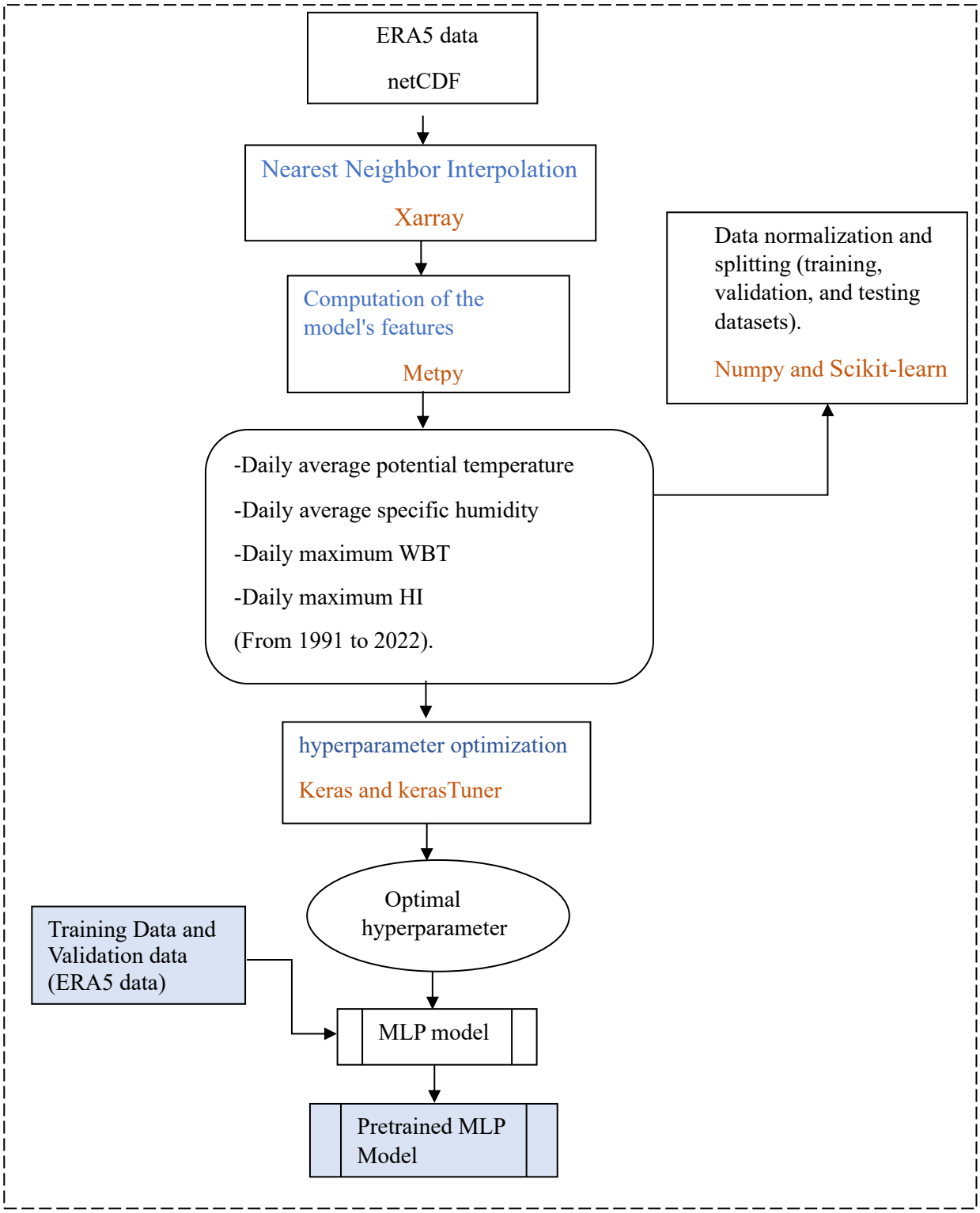

Figure 9: Methodology to implement the MLP model with ERA5 data.

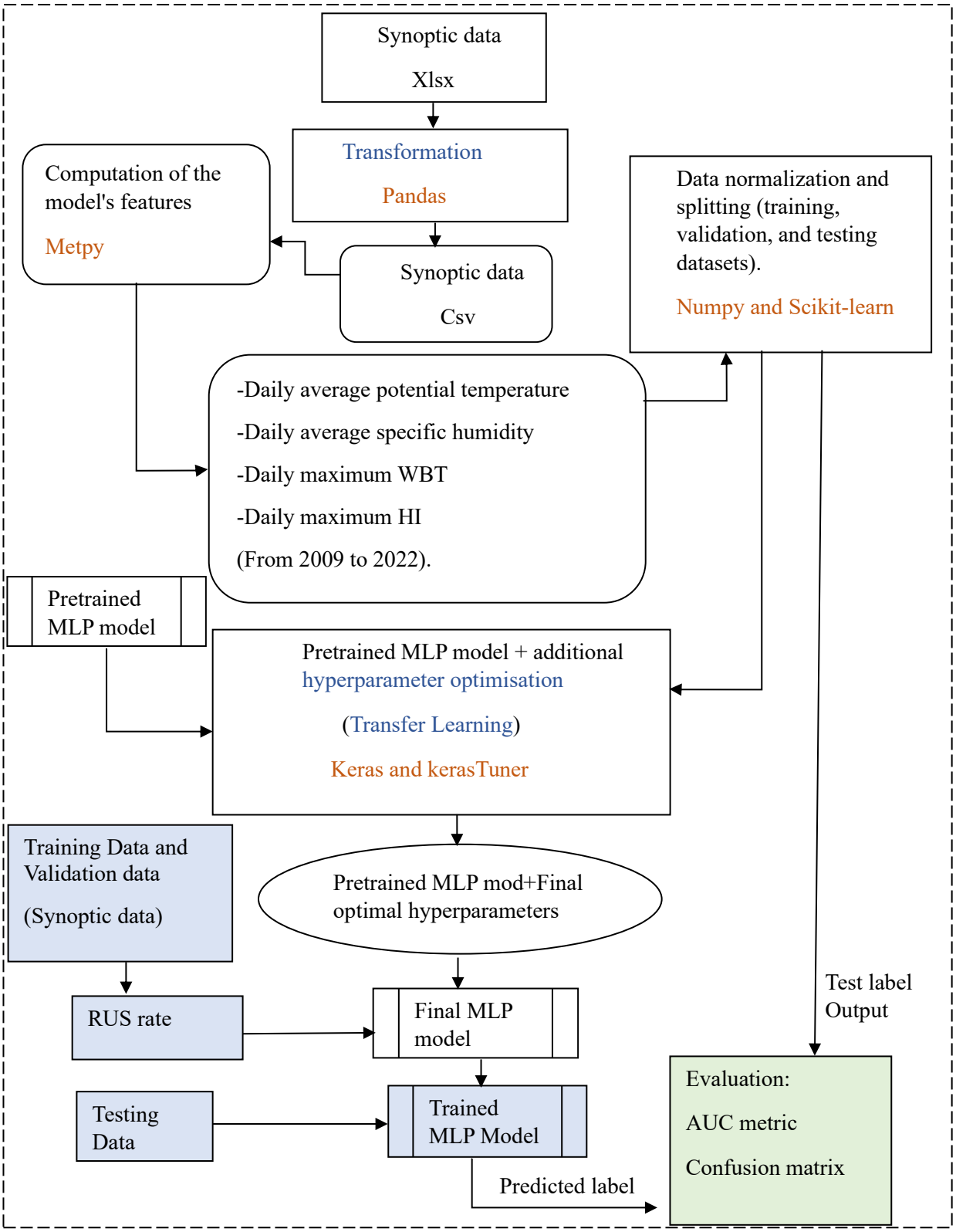

Figure 10: Methodology for Implementing the MLP Model through TL with Synoptic Data

2.4.4.1 Hyperparameter Optimisation

The performance of ML or DL algorithms largely relies on selecting a good collection of hyperparameters. However, with the vast range of possible hyperparameter combinations, it becomes challenging and time-consuming for human experts to manually tune them.

The goal of optimisation in ML is to find the optimal combination of hyperparameters that maximizes performance on a given task. Employing optimisation methods enable to efficiently explore the hyperparameter space of an ML model, thereby improving its performance and reducing the manual effort required in hyperparameter tuning. One strong argument for employing Bayesian optimisation in this study for our MLP optimisation is due to its ability to outperform human expertise and lead to significant improvements in model performance (Snoek et al., 2012).

There are numerous approaches to optimizing an ML model. KerasTuner, a scalable and user-friendly hyperparameter optimisation framework, was used in our case. KerasTuner is an open-source Python library that is useful because it helps in setting hyperparameters in a sensible and practical way. Figure 11 illustrates the fundamental principle of hyperparameter optimisation.

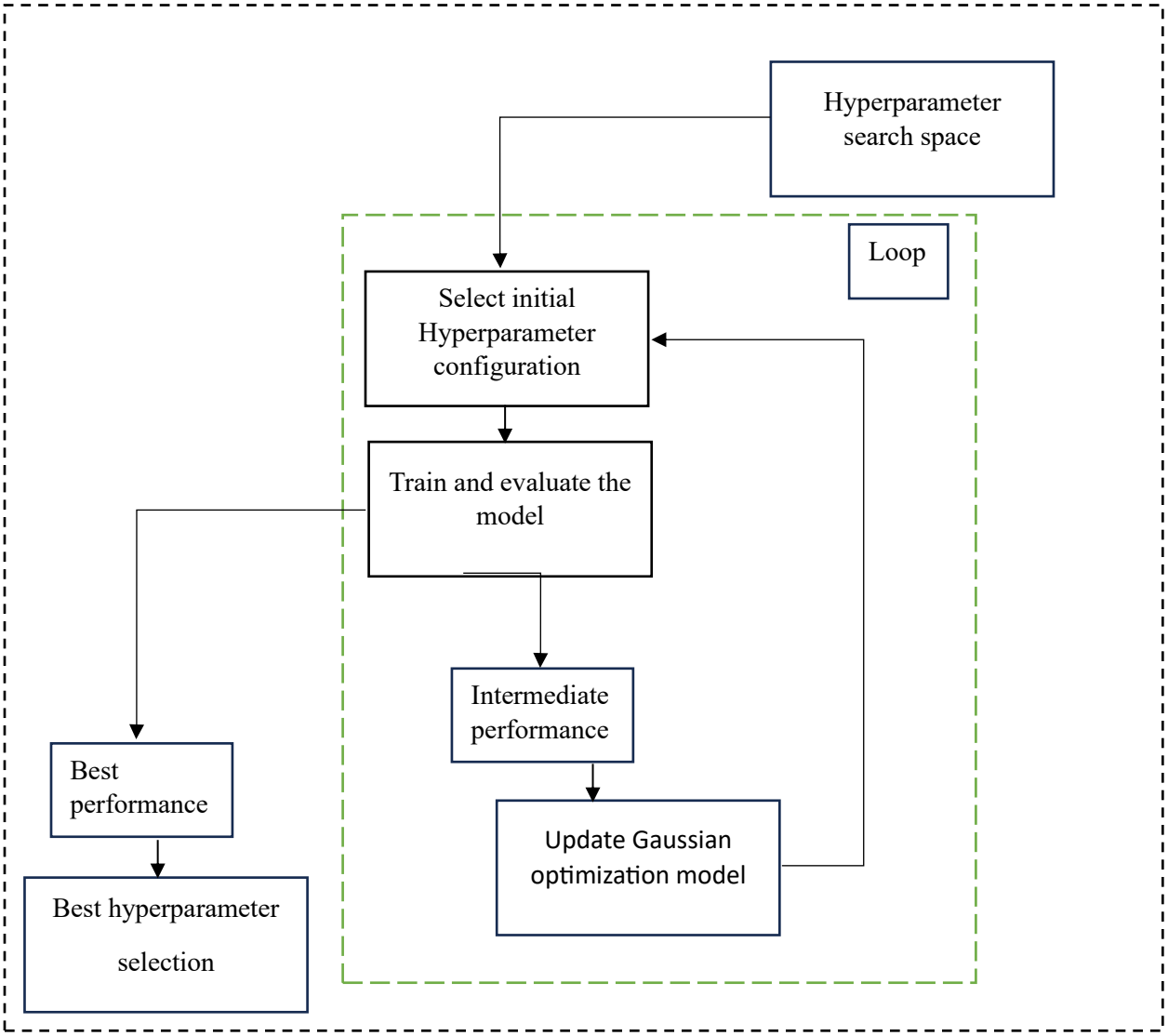

Figure 11: Fundamental principle of Bayesian optimization

In our study framework, the hyperparameters include units representing the number of neurons in each dense layer, regularization rates for controlling overfitting, dropout rates for regularization and preventing overfitting, and the learning rate which is for controlling the step size during optimisation. Each hyperparameter is defined within a specific range and step size, allowing the search algorithm to explore different combinations and find the best configuration for the model. The tables below provide an overview of the hyperparameters and their corresponding search spaces. They show the possible values that were explored during the hyperparameter tuning process to optimize the MLP models.

Table 1**:** Hyperparameter space of the pretrained MLP model

Hyperparameter	Range	Step	Distribution
unit_1	256 - 512	16	Integer
unit_2	128-256	16	Integer
unit_3	64-128	16	Integer
reg_rate_3	[0.001, 0.002, 0.003]	-	Categorical
unit_4	32-64	8	Integer
reg_rate_4	[0.01, 0.02, 0.03]	-	Categorical
drop_rate_1	0.0 - 0.5	0.1	Float
unit_5	8 - 32	2	Integer
reg_rate_5	[0.001, 0.002, 0.003]	-	Categorical
drop_rate_2	0.0 - 0.5	0.1	Float
Learning rate	[1e-4, 1e-1] (log scale sampling)		Float

Table 2**:** Hyperparameter space of the final MLP model

Hyperparameter	Range	Step	Distribution
unit_1	129-256	4	Integer
unit_2	64-128	4	Integer
unit_3	30-62	2	Integer
unit_4	16-28	2	Integer
unit_5	8-14	2	Integer
Learning_rate	[1e-4, 1e-1] (log scale sampling)	-	Float

Let us proceed with an overview of the tables and provide a detailed explanation of each component.

Hyperparameter: This column denotes the name assigned to the hyperparameter under consideration within the hyperparameter search space. It serves as an identifier for the specific parameter being optimized.

Range: The range column specifies the boundaries of values that the hyperparameter is allowed to take. It defines the lower and upper limits within which the hyperparameter can vary during the optimization process.

Step: The step column denotes the increment or step size between consecutive values within the defined range. It determines the granularity of the hyperparameter search space by specifying the magnitude of change between each value.

Distribution: The distribution column provides information about the nature of values that the hyperparameter can assume. This table distinguishes between three types of distributions:

- Integer: If the hyperparameter is labelled as an integer distribution, it signifies that only whole number values within the specified range are considered.

- Categorical: Categorical distributions refer to hyperparameters that can only take specific pre-defined categorical values mentioned in the table. These values are explicitly listed and serve as the options to be explored.

- Float: When a hyperparameter is categorized as a float distribution, it implies that the parameter can assume continuous floating-point values within the defined range.

By exploring different values within the defined ranges, the hyperparameter tuning process aims to find the optimal combination of hyperparameter values that maximizes the desired metric.

2.4.4.2 Presentation of the data

Table 3**:** MLP Input and Output Data Presentation

Period	MLP input features			Output state	
Date	**Potential temperature**	**Specific humidity**	**Wet bulb temperture**	**Cell_1**	**Cell_2**
Day	Feature value	Feature value	Feature value	Q_1	Q_2

According to the Table 3, the dataset utilized for constructing the MLP models can be categorized into three distinct sections.

The first section pertains to the timeframe encompassing the entire dataset, denoted as the Period section. This section defines the temporal scope of the data in terms of daily data, which, as

indicated before in this section, varies depending on the dataset used. Specifically, for this study, the ERA5 dataset spans from January 1, 1991, to December 31, 2022, while the Synoptic data covers the period from January 1, 2009, to December 31, 2022.

The subsequent section concerns the input characteristics of the MLP model. This section of the dataset assumes paramount importance within the MLP model framework, as it serves as the fundamental element for analysis and prediction purposes. The features encompassed in this segment of the data encapsulate pertinent attributes that exert significant influence on the target variable under consideration. These input features are systematically organized in a tabular format, wherein each row denotes an individual instance or sample for each day, and each column corresponds to a distinct feature as shown in Table 3. This structured arrangement enables the MLP model to effectively process and scrutinize the provided data.

The last section is about the output or target of the MLP model. In the context of this supervised learning task, the labelled target variable signifies the intended output or true value corresponding to each input instance. It comprises discrete categories or labels denoted as q1 and q2 in Table 3. These categories possess a binary characteristic, implying that each category can take on one of two distinct values, namely 0 or 1. In our specific case, the value [1 0] signifies the occurrence of an HD, while [0 1] corresponds to a normal day.

2.4.4.3 Data processing

Data processing is a crucial and indispensable step in building any machine or DL model. It plays a vital role in transforming raw data into a suitable format that can be effectively utilized as input for the model. Proper data processing significantly impacts the model's performance and generalization capabilities. The data processing step encompasses several crucial tasks, starting with data cleaning, where missing values, outliers, and inconsistencies are addressed to prevent potential distortions in the learning process. Next, the dataset is split into training, validation, and testing sets. The training set is used to optimize the model's parameters, while the validation set aids in tuning hyperparameters and assessing the model's performance during training. Finally, the testing set serves as an independent evaluation to estimate the model's true performance on unseen data. By using different sets for training and testing, data processing ensures that the model

generalizes well to new, unseen samples. Another crucial aspect of data processing is normalization, which standardizes the numerical features to a common scale.

2.4.4.3.1 Data splitting

The data splitting process in this study was conducted using sklearn.model_selection module from the scikit-learn library. This module offers an efficient and scientifically rigorous approach to dividing the dataset into training, validation, and testing subsets. For the MLP built using the ERA5 dataset (pre-trained model), the dataset was partitioned into 6934 samples for training, which corresponds to an approximate duration of 19 years, 2973 samples for validation, approximately representing 8 years, and finally 1749 samples, corresponding to approximately 4 years, for testing purposes. On the other hand, for the MLP built using the Synoptic data, the dataset was divided into 2475 training samples, equivalent to a span of 7 years of data. Additionally, 1062 validation samples were used, representing a duration of 3 years of daily data. Furthermore, 625 samples were allocated for testing, which encompassed a period of 2 years of data.

2.4.4.3.2 Data normalization

Additionally, the normalization technique employed to preprocess the data was the min-max scaling method. The min-max scaling transforms the values of each feature in the dataset to a range between 0 and 1, preserving the original relationships between data points while ensuring that all features have a uniform scale. By applying this technique, the model is less likely to be influenced by features with larger magnitude values, preventing potential biases and instabilities during training. The sklearn.preprocessing module of the scikit-learn library was utilized to implement the min-max scaling method, ensuring consistency and efficiency in the normalization process across both the ERA5 and Synoptic datasets.

$$m = \frac{X - X_{min}}{X_{max} - X_{min}} \quad \text{(Eq 16)}$$

m is our new value

X is the original cell value

X_{min} is the column's minimum value

X_{max} is the maximum value of the column

2.4.4.4 Class-size imbalance and undersampling

Classes are imbalanced by construction for the prediction of unusual events. Class imbalance is a prevalent issue for machine and DL models. It arises when the distribution of examples within a dataset is heavily skewed or biased toward one class. This situation creates considerable issues for predictive modeling since algorithms are affected by the majority class and fail to appropriately represent the minority class. The decrease in model performance is one of the key consequences of class imbalance (Miroslav & Matwin, 1997). When the majority class dominates the dataset, machine and DL algorithms tend to prioritize accuracy over capturing the minority class. As a result, the model may be biased toward the majority class, resulting in a poor predicted performance for the minority class (Longadge et al., 2013). This can be particularly problematic in applications where the minority class is of significant interest, such as the prediction of unusual events.

In our study, we propose to address the issue of class imbalance in the training of our Multilayer Perceptron (MLP) model by utilizing the Random Under-Sampling (RUS) method. The objective is to mitigate the impact of class imbalance by reducing the disproportionate representation of the minority class during the model training process. By employing RUS, we aim to create a more balanced dataset, which can improve the ability of the model to learn from both classes effectively. The RUS method works by randomly selecting a subset of instances from the majority class (the overrepresented class) to match the size of the minority class (the underrepresented class). This approach involves removing instances from the majority class until the desired balance between the classes is achieved. This way, the training dataset becomes more balanced, allowing the MLP model to learn from both classes more accurately. The goal of RUS is not to discard all instances of the majority class, but to create a more equitable representation that mitigates the dominance of the majority class during training. The concept of the RUS rate refers to the percentage of examples from the majority class that will be eliminated during the under-sampling process. This rate determines the degree to which the class imbalance is mitigated. For example, a RUS rate of 0.10 implies that 10% of the instances from the majority class will be removed, whereas a rate of 1

indicates the complete elimination of excessive instances from the majority class. By adjusting the RUS rate, we can explore different levels of class imbalance reduction and examine their impact on the model's prediction performance. In our study, we have explored the impact of different RUS ratios on the prediction performance of the MLP model. Initially, the MLP model was optimized using the normal training dataset without any RUS method applied. Subsequently, four additional MLP models were trained after applying RUS rates of 0.25, 0.5, 0.75, and 1 to the training dataset. This approach allowed us to investigate how different levels of class imbalance reduction affect the model's predictive capabilities. By systematically varying the RUS rate, we aimed to identify the optimal balance between class representation and prediction performance for our specific problem. By utilizing the RUS method and evaluating different RUS ratios, our study aims to provide insights into the impact of class imbalance mitigation techniques on MLP model training and prediction performance. This approach contributes to the understanding of how to address the challenges posed by imbalanced datasets and enhance the effectiveness of the MLP model in handling such scenarios. The figure below shows the class proportion after applying the different RUS rate.

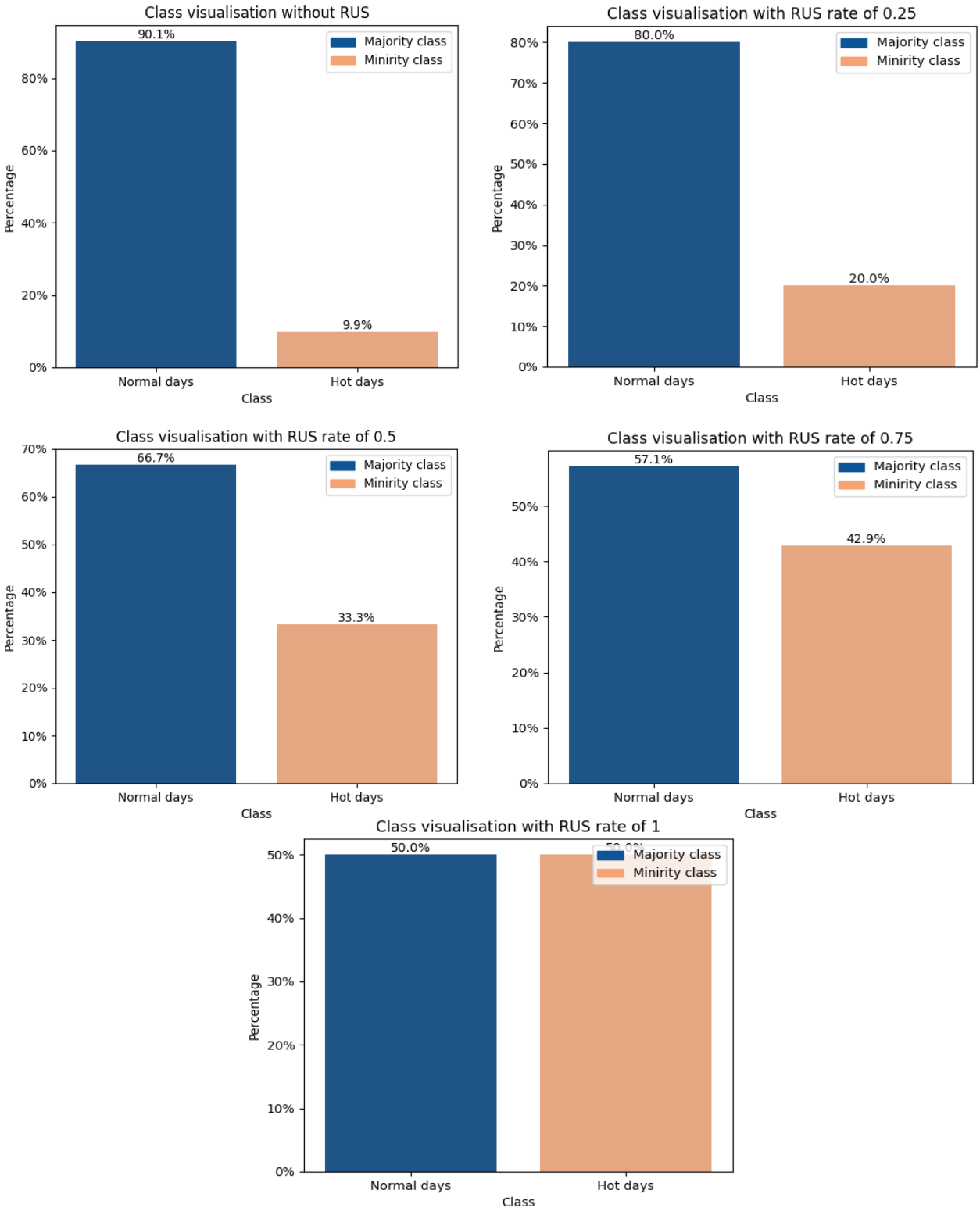

Figure 12: Visualizing Different Random Undersampling Rates Applied to Synoptic Training Data.

2.4.4.5 Performance assessment

A performance assessment approach based on the confusion matrix for two classes was employed to evaluate the effectiveness of the predictive model for HD occurrences (see Table 4). The primary objective of this assessment is to determine the ability of the MLP to accurately classify instances of HDs based on the provided input features.

A set of carefully defined evaluation metrics was used to assess the performance of the model. Given the imbalanced nature of the problem, where HDs are scarce compared to non-HDs, exploration was conducted regarding the utilization of the Area Under the Curve (AUC) metric. The AUC metric is widely recognized as a robust measure for assessing binary classification models in imbalanced scenarios (Branco et al., 2015), as it takes into account both true positive rates (TPR) and false positive rates (FPR) across varying classification thresholds. The TPR, also known as sensitivity or recall, represents the proportion of correctly identified HDs out of the total actual HDs. By incorporating TPR into our performance assessment, we were able to evaluate the ability of the model to capture and correctly classify instances of HDs. In addition to TPR, we also considered the FPR, which quantifies the proportion of falsely identified non-HDs among the total actual non-HDs. The inclusion of FPR allowed us to assess the specificity of the model and its potential for false alarms when predicting HD occurrences.

$$\mathrm{TPR} = \frac{\mathrm{TP}}{\mathrm{TP} + \mathrm{FN}} \qquad \text{(Eq 17)}$$

$$\mathrm{FPR} = \frac{\mathrm{FP}}{\mathrm{TN} + \mathrm{FP}} \qquad \text{(Eq 18)}$$

TP: the number of True Positives

TN: the number of True Negatives

FP: the number of False Positives

FN: the number of False Negatives

Table 4**:** Confusion matrix for two class problem.

		PREDICTED LABEL	
		Positive	Negative
TRUE LABEL	Positvive	TPR(%)	FNR(%)
	Negative	FPR(%)	TNR(%)

The choice of only commenting on the TPR and FPR is justified by the relationship between these metrics and their complement counterparts, the False Negative Rate (FNR) and the True Negative Rate (TNR) respectively. As TPR + FNR = 1 and FPR + TNR = 1, these pairs of metrics are inversely related and provide redundant information. Therefore, by focusing solely on the TPR and FPR, we can efficiently examine the model's performance without repeating information and maintaining a simple and focused analysis.

Chapter 3: Results and Discussion

This section serves to present the principal findings derived from our study. Firstly, an analysis of the temporal distribution of HWs in Abidjan, categorized by month, will be provided, along with the prediction results obtained from both the pre-trained and final Multilayer Perceptron (MLP) models. Each individual result will be subject to a comprehensive discussion aimed at elucidating the extent to which the obtained findings conform to or deviate from the existing body of research.

3.1 Temporal analysis of hot days and heat waves over Abidjan based on the heat index indicator

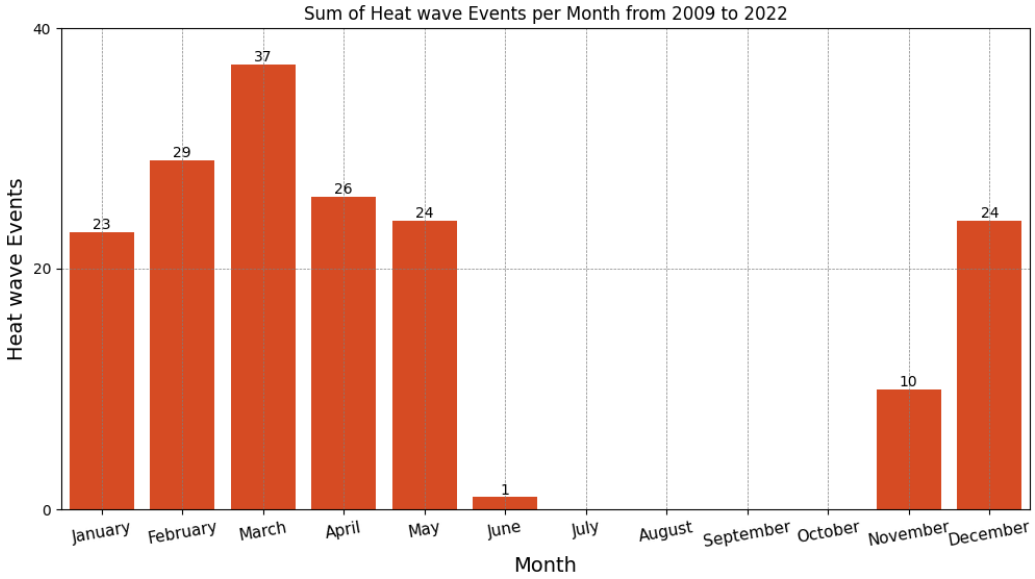

Figure 13: Frequency of HW occurrences per month in Abidjan during the last past 13 years

The examination of HW occurrences in Abidjan, capital of Côte d'Ivoire, based on the HI computed with synoptic data from 2009 until 2022, showed in Figure 13 reveals interesting trends and variations. The result focuses on the monthly distribution of HWs, revealing patterns and characteristics of these extreme weather phenomena. Examining the general trend, it is clear that HWs in Abidjan city exhibit seasonal fluctuations throughout the year. The months with most HWs are March, February, and April, with 37, 29, and 26 occurrences, respectively during the past 13 years. These findings align with the research conducted by RINGARD J et al., (2014), which emphasizes that the period between January and March constitutes the hottest season in Abidjan, further substantiating the validity and reliability of our respective investigations. When compared

to other months, these months have a higher frequency of HWs. In Abidjan, March looks to be the most active month for HW occurrences. In contrast, HWs were absent in June, July, August, September, and October, with zero occurrences over the 13-year period. These months consistently show a lower probability of HWs occurrences. This result implies that HW occurrences in Abidjan has a distinct seasonal pattern, with the summer months having a reduced risk.

The observed trends in HW occurrences in Abidjan city can be attributed to several factors. First and foremost, the geographical location of Abidjan within the tropical climate zone plays a crucial role. The city is situated close to the equator, which results in relatively high temperatures throughout the year. This, combined with the presence of the Atlantic Ocean, leads to increased moisture availability and influences local weather patterns (Guigma et al., 2020). The months with the highest occurrences of HWs (March, February, and April) coincide with the transition from the dry season to the rainy season in Abidjan. During this period, the region experiences a buil-dup of heat, as solar radiation intensifies and the moisture content gradually increases. These conditions create a conducive environment for the formation of HWs. Furthermore, the urban heat island effect may contribute to the higher occurrences of HWs in Abidjan. As a rapidly growing urban centre, Abidjan experiences significant urbanization, resulting in increased impervious surfaces and reduced vegetation cover. These changes lead to enhanced heat absorption and limited natural cooling mechanisms, amplifying the intensity and duration of HWs within the city (Li et al., 2022).

3.2 Evaluating the Performance of the Pre-trained MLP Model with ERA5 Data.

In this section, we will dive into the full presentation of the results obtained from the pre-trained optimal MLP model. This model has undergone thorough training, validation, and testing processes using daily ERA5 data covering the period from 1991 to 2022. By analysing these results, we aim to provide insight into the model's performance, its ability to capture patterns and trends in the data, and its overall effectiveness in handling HDs prediction.

3.2.1 Evolution of the training and validation step

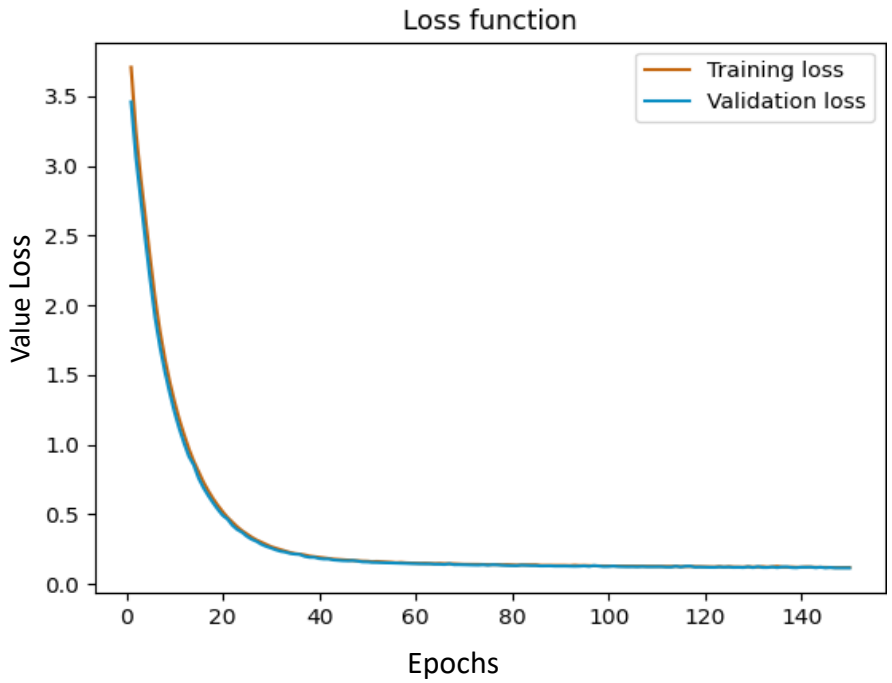

Figure 14: Evaluation of Pre-trained MLP loss Function during the training and validation

Based on the training and validation curves (Figure 14), it is evident that the binary cross entropy chosen as loss function for this model consistently exhibited convergence over the entire duration of 150 epochs. This indicates a robust training process, where the model effectively learned complex patterns and features associated with HD classification. The closed nature of both curves signifies the ability of the model to generalize well to unseen data, as the validation curve closely tracks the training curve without evidence of overfitting (Jeff Heaton, 2018). This result underscore the effectiveness of the chosen loss function in guiding the training process, yielding refined predictions, and improved overall performance.

3.2.2 Analysis of Hot Day Prediction Results using Pre-trained MLP Model over the ERA5 data

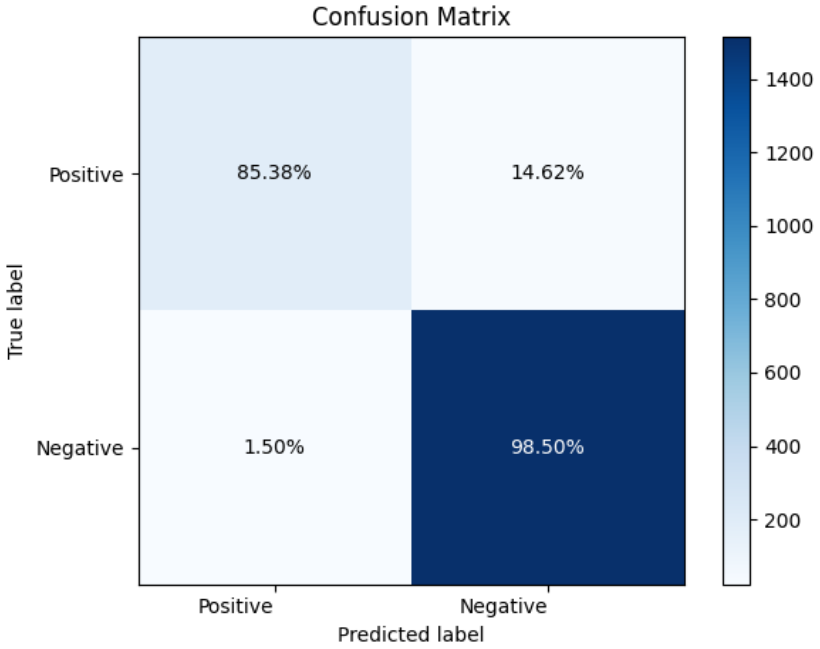

Figure 15: Confusion matrice showing the pre-trained MLP model performance

The obtained TPR score of 85.38% indicates that the model accurately detected a portion of the actual HDs over the 4-year period (Figure 15). This high TPR demonstrates the model's effectiveness in identifying true positive cases, which is valuable for applications like HW prediction and resource allocation. However, it is worth noting that there may still be instances where the model fails to identify HDs, resulting in false negatives. False negatives occur when positive instances (e.g., HDs) are incorrectly classified as negatives (e.g., non-HDs). Such misclassifications can have consequences, potentially leading to inadequate actions or measures for warm weather conditions.

Furthermore, the model exhibited a low FPR of 1.50%, indicating its ability to minimize false alarms characterised by predicting HDs when they did not occur. A lower FPR is desirable as it reduces the number of false positive predictions, thereby minimizing unnecessary actions or resource allocation triggered by false alarms. The low FPR of 1.50% of the model reflects its good specificity and proficiency in distinguishing between hot and non-HDs.

These metrics indicate the potential of the model as a pre-trained model for TL. Trained and validated on 19 years and 8 years of data respectively, the model has acquired extensive experience in detecting HD occurrences. This accumulated knowledge can be leveraged to develop a final model capable of adapting to the synoptic data environments, which potentially have fewer HD occurrences (Lu et al., 2015). The proficiency of the pre-trained model in recognizing patterns may be used to improve performance adaptation. Harnessing its extensive training, the final model is may demonstrate enhanced accuracy and generalization in detecting HDs, even with limited occurrences (Zhu et al., 2011).

3.3 Analysis of Hot Day Prediction Results Using Optimal MLP Models and Various Random Under-Sampling Strategies

As previously discussed in the methodology part, different random under-sampling (RUS) strategies have been applied to the imbalance dataset to attain the desired ratio or proportion between the minority and majority classes. Following the different RUS scenarios characterized by the class rate, a succession of predictions by the optimized final MLP models were performed.

This section is attended to present the results obtained from predicting HDs using various optimized MLP models on the different under-sampling scenarios previously discussed.

The graphs below represent the confusion matrix from the HD's prediction with the optimal MLP models on the test synoptic station dataset.

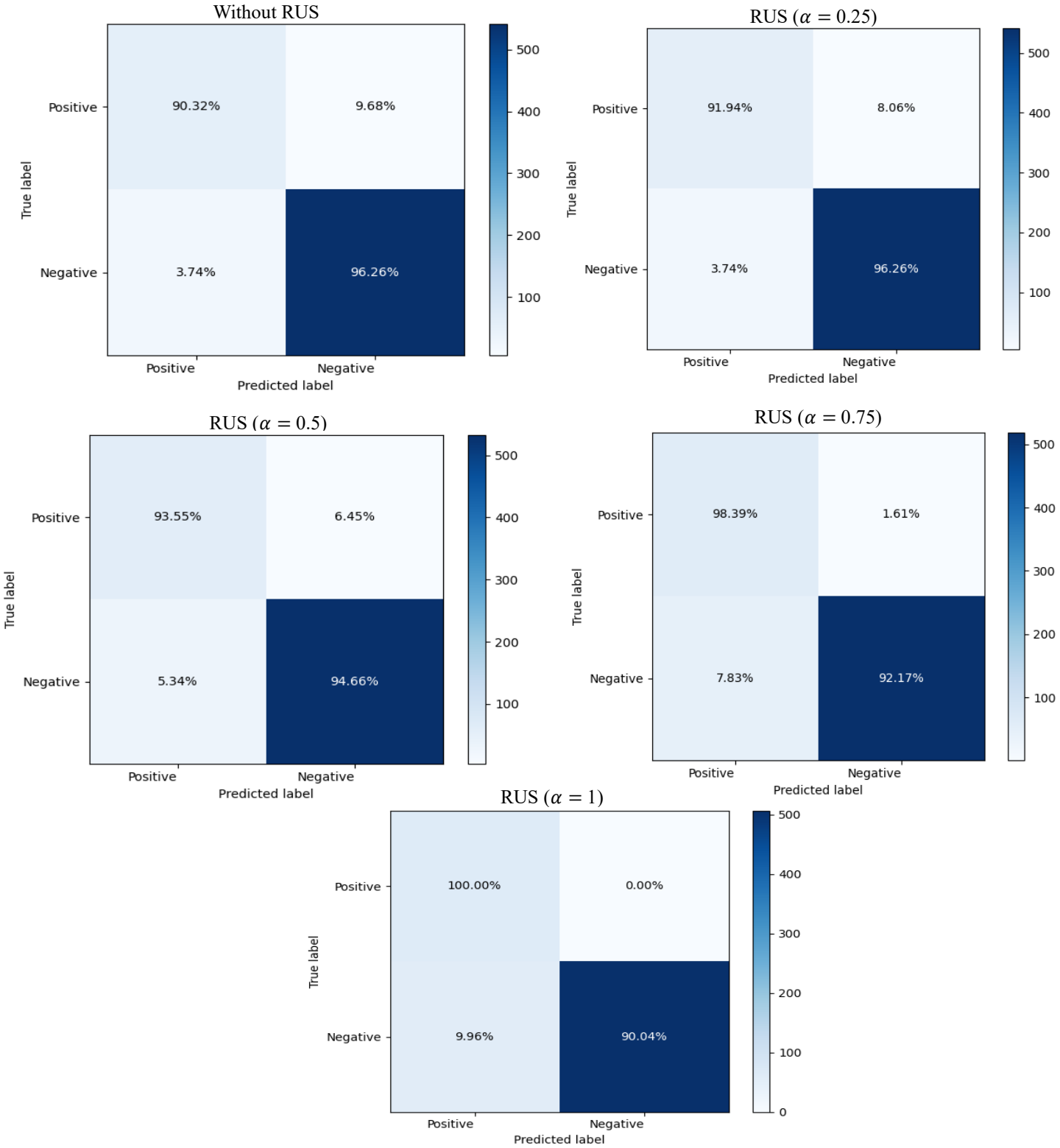

Figure 16: Performance of the models with respect to the RUS rate.

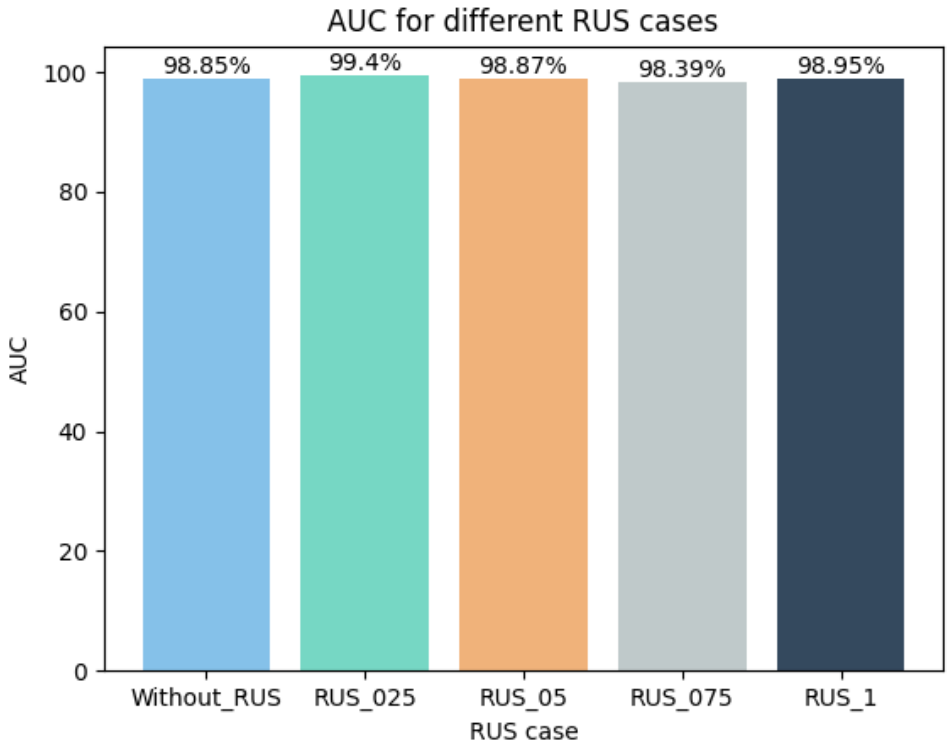

Figure 17: AUC metric for the different under-sampling rate

By analyzing the result displayed in the figure above (Figure 16), it becomes evident that as the count of non-HDs diminishes in the training data, which result from an increase in the RUS rate, the MLP model adjusts its predictions accordingly. As the RUS increases from 0.25 to 1, the TPR exhibits an increasing trend. This observation suggests that reducing the presence of HDs in the training data enhances the model's ability to accurately detect occurrences of HDs. This is manifested by TPR values ranging from 90.32% without resorting to under-sampling of training data up to 100% which corresponds to an under-sampling rate value of 1.

Similarly, as the rate of under-sampling increases, so does the false positive rate (FPR). This is justified by the different increasing values of the false positive rate in the results, from 3.74% without any under-sampling method to 9.96% with an under-sampling rate of 1 (Figure 16). This result signifies that as the number of non-HDs is reduced in the training set, the MLP (Multilayer Perceptron) increases its predictions of false occurrences of HDs.

As depicted in Figure 17 above, the AUC values for each scenario of the under-sampling method do not display a clear correlation with the under-sampling rate. However, It is worth noting that

the values of the AUC metric vary slightly across the scenarios, but all consistently indicate the good overall ability of the models to discriminate between hot and cold days. Also, the AUC metric of the scenario without any under-sampling method yields a value of 98.85% which is greater than the scenario with the under-sampling rate of 0.75 which instead yield an AUC value of 98.39%. The other under-sampling rate scenario all provide AUC values above 98.50% with the highest AUC value appearing for the under-sampling rate scenario of 0.25 which obtained a value of 99.4%.

The observation that the True Positive Rate (TPR) increases as the under-sampling rate increases can be explained by the impact of under-sampling on the class distribution within the training dataset. When the under-sampling rate is low, the majority class instances far outweigh the minority class instances, resulting in a data imbalance. This then results in a lower TPR as the model may struggle to effectively learn the patterns and characteristics of the minority class, leading to a higher number of false negatives (Johnson & Khoshgoftaar, 2020).

Under-sampling involves reducing the number of instances from the majority class to balance it with the number of instances from the minority class. By increasing the under-sampling rate, we are essentially reducing the dominance of the majority class in the training dataset, resulting in a more balanced dataset where the positive instances (HDs) are adequately represented (Branco et al., 2015).

The advantage of this approach is that it allows the model to capture and learn from a greater number of positive instances. By having more HD instances in the training dataset, the model has a higher chance of encountering a variety of scenarios and conditions that lead to HDs. This exposure allows the model to capture the diverse range of patterns and correlations associated with HDs. For example, the model has more chances to learn that specific combinations of the input features tend to coincide with HDs, such as the potential temperature, specific humidity, and WBT.

Additionally, with a larger representation of HDs, the model can uncover rare or uncommon patterns that might have been overlooked when the positive instances were scarce in the training dataset without any under-sampling method. The increased exposure helps the model identify nuanced relationships and interactions among features that might have a significant impact on the

occurrence of HDs. These insights can enhance the model's ability to accurately predict HDs by recognizing the complex interplay between the input feature values and their combined influence on the occurrence of HDs. Consequently, the model's ability to identify and predict HDs is enhanced.

On the other hand, when analysing the impact of increasing the under-sampling rate on model performance, it is crucial to consider its implications for the False Positive Rate (FPR) and overall accuracy. Figure 16 clearly demonstrates that as the under-sampling ratio increases across different scenarios, the FPR exhibits an increasing trend. This happens because diminishing the dominance of the majority class through under-sampling reduces the amount of instances from that class, which might lead to misclassifying instances as positive and affecting the model's overall performance.

The distribution of the AUC metric in Figure 17 further emphasizes this trend. The scenario with an under-sampling rate of 0.25 achieves the highest AUC (Area Under the Curve) score compared to other scenarios, indicating excellent predictive capability. In this scenario, the TPR is 91.94% while the FPR remains constant at 3.74%, reflecting a successful capture of positive instances with a relatively low rate of falsely labelling negative instances as positive. As the under-sampling rate increases to 0.5, 0.75, and 1, the TPR continues to improve, reaching 93.55%, 98.39%, and 100% respectively. However, with this increase, the FPR also rises. The scenarios with under-sampling rates of 0.75 and 1 exhibit higher FPR values of 7.83% and 9.96% respectively, indicating a higher proportion of falsely labelled negative instances. Consequently, there is a slight decrease in AUC compared to the scenario with an under-sampling rate of 0.25.

This investigation aligns with the outcomes reported by (Jacques-Dumas et al., 2022), highlighting the vulnerability of the model to misclassifying non-HDs as HDs when exposed to an elevated under-sampling rate in the training data, consequently hindering its overall performance.

Conclusion and perspectives

Finally, this study makes an important contribution to the use of AI in HW prediction in West Africa, notably in the setting of Abidjan, the capital of Cote d'Ivoire. It is one of the first research over this specific area that leverages AI approaches for HWs prediction.

The study conducted a temporal investigation of HW occurrences in Abidjan from 2009 to 2022, shedding light on the seasonal beheviour observed during this period by this extreme event. Notably, the month of March emerged as the month with the highest frequency of HW occurrences, while June, July, August, September and October exhibited a lower probability of HW events. This result confirms that HW occurrences exhibit a specific temporal pattern.

Furthermore, the potential of using ANNs, specifically the Multilayer Perceptron (MLP) model, for predicting HW occurrences in Abidjan has been explored. Our analysis primarily utilized potential temperature, specific humidity, and wet bulb temperature as input variables. To address the imbalanced datasets resulting from the scarcity of Hot Days (HDs) in the training dataset, TL and RUS techniques were employed. The findings revealed that the MLP model, in conjunction with TL and under-sampling, achieved remarkable performance in predicting HWs thereby predicting the individual hot days. The performance of the MLP models was evaluated using the Area Under the Curve (AUC) metric, and all models trained with different under-sampling rates demonstrated good AUC performance.

Overall, this study contributes to HW prediction in West Africa and provides useful information for policymakers and stakeholders in effectively managing HW events in Abidjan and other similar regions. While our research has provided valuable insights into improving the operational predictability of HWs in Abidjan, it is important to acknowledge the limitations of our study. These limitations serve as avenues for future research and improvement:

- Data Availability: The effectiveness of our MLP model heavily relies on the availability and quality of the input data. In our case, the availability and accessibility of comprehensive datasets, including geographical information, were limited. Future studies should focus on acquiring more extensive and accurate datasets to enhance the accuracy and reliability of the predictions.

- Generalizability: Our study focused specifically on the case study of Abidjan, and the applicability of our findings to other developing countries and cities may be limited. It is crucial to conduct similar investigations in various geographical locations and climates to validate the robustness and generalizability of such developed models.
- Model Optimization: Although our MLP model demonstrated promising results, there is always room for improvement in terms of model architecture, hyperparameter tuning, and optimization techniques. Further exploration of advanced neural network architectures, such as convolutional neural networks (CNNs) or recurrent neural networks (RNNs), may yield more accurate and efficient predictions and also allow to extend the leadtime for the prediction.

By addressing these limitations and pursuing these future perspectives, researchers, and policymakers can further advance the operational predictability of HWs in developing countries, ultimately contributing to the protection of vulnerable populations and the development of effective climate resilience strategies.

Bibliographies:

Ahoussi, K. E., Koffi, Y. B., Kouassi, A. M., Soro, G., & Soro, N. (2013). Étude De La Variabilité Hydroclimatique Et De Ses Conséquences Sur Les Ressources En Eau Du Sud Forestier Et Agricole De La Côte d'Ivoire: Cas De La Région d'Abidjan-Agboville. International Multilingual Journal of Contemporary Research, 1(1).

Barbier, J., Guichard, F., Bouniol, D., Couvreux, F., & Roehrig, R. (2018). Detection of Intraseasonal Large-Scale Heat Waves: Characteristics and Historical Trends during the Sahelian Spring. Journal of Climate, 31(1), 61–80. https://doi.org/10.1175/JCLI-D-17-0244.1

Batté, L., Ardilouze, C., & Déqué, M. (2018). Forecasting West African Heat Waves at Subseasonal and Seasonal Time Scales. Monthly Weather Review, 146(3), 889–907. https://doi.org/10.1175/MWR-D-17-0211.1

Branco, P., Torgo, L., & Ribeiro, R. (2015). A Survey of Predictive Modelling under Imbalanced Distributions (arXiv:1505.01658). arXiv. http://arxiv.org/abs/1505.01658

BNETD (2008) 'Impact environnemental et social de la mise en œuvre des périmètres de protection autour des points de captage d'eau souterraine du District d'Abidjan.', Rapport Définitif février 2008., p. 97.

Campbell, S., Remenyi, T. A., White, C. J., & Johnston, F. H. (2018). Heatwave and health impact research: A global review. Health & Place, 53, 210–218. https://doi.org/10.1016/j.healthplace.2018.08.017

Chen, K., Horton, R. M., Bader, D. A., Lesk, C., Jiang, L., Jones, B., Zhou, L., Chen, X., Bi, J., & Kinney, P. L. (2017). Impact of climate change on heat-related mortality in Jiangsu Province, China. Environmental Pollution, 224, 317–325. https://doi.org/10.1016/j.envpol.2017.02.011

Coumou, D., & Rahmstorf, S. (2012). A decade of weather extremes. Nature Climate Change, 2(7), 491–496. https://doi.org/10.1038/nclimate1452

Déqué, M., Calmanti, S., Christensen, O. B., Dell Aquila, A., Maule, C. F., Haensler, A., Nikulin, G., & Teichmann, C. (2017). A multi-model climate response over tropical Africa at +2 °C. Climate Services, 7, 87–95. https://doi.org/10.1016/j.cliser.2016.06.002

Di Napoli, C., Pappenberger, F., & Cloke, H. L. (2019). Verification of Heat Stress Thresholds for a Health-Based Heat-Wave Definition. Journal of Applied Meteorology and Climatology, 58(6), 1177–1194. https://doi.org/10.1175/JAMC-D-18-0246.1

Diallo, I., Bain, C. L., Gaye, A. T., Moufouma-Okia, W., Niang, C., Dieng, M. D. B., & Graham, R. (2014). Simulation of the West African monsoon onset using the HadGEM3-RA regional climate model. Climate Dynamics, 43(3–4), 575–594. https://doi.org/10.1007/s00382-014-2219-0

Do Carmo Nicoletti, M., & Jain, L. C. (Eds.). (2009). Computational Intelligence Techniques for Bioprocess Modelling, Supervision and Control (Vol. 218). Springer Berlin Heidelberg. https://doi.org/10.1007/978-3-642-01888-6

Engdaw, M. M., Ballinger, A. P., Hegerl, G. C., & Steiner, A. K. (2022). Changes in temperature and heat waves over Africa using observational and reanalysis data sets. International Journal of Climatology, 42(2), 1165–1180. https://doi.org/10.1002/joc.7295

Fachantidis, A., Partalas, I., Tsoumakas, G., & Vlahavas, I. (2013). Transferring task models in Reinforcement Learning agents. Neurocomputing, 107, 23–32. https://doi.org/10.1016/j.neucom.2012.08.039

Fischer, E. M., & Schär, C. (2010). Consistent geographical patterns of changes in high-impact European heatwaves. Nature Geoscience, 3(6), 398–403. https://doi.org/10.1038/ngeo866

Fontaine, B., Janicot, S., & Monerie, P.-A. (2013). Recent changes in air temperature, heat waves occurrences, and atmospheric circulation in Northern Africa: HEAT WAVES AND ATMOSPHERIC CIRCULATION. Journal of Geophysical Research: Atmospheres, 118(15), 8536–8552. https://doi.org/10.1002/jgrd.50667

Fouillet, A., Rey, G., Laurent, F., Pavillon, G., Bellec, S., Guihenneuc-Jouyaux, C., Clavel, J., Jougla, E., & Hémon, D. (2006). Excess mortality related to the August 2003 heat wave in France. International Archives of Occupational and Environmental Health, 80(1), 16–24. https://doi.org/10.1007/s00420-006-0089-4

Giorgi, F., Coppola, E., Raffaele, F., Diro, G. T., Fuentes-Franco, R., Giuliani, G., Mamgain, A., Llopart, M. P., Mariotti, L., & Torma, C. (2014). Changes in extremes and hydroclimatic regimes in the CREMA ensemble projections. Climatic Change, 125(1), 39–51. https://doi.org/10.1007/s10584-014-1117-0

Guigma, K. H., Todd, M., & Wang, Y. (2020). Characteristics and thermodynamics of Sahelian heatwaves analysed using various thermal indices. Climate Dynamics, 55(11–12), 3151–3175. https://doi.org/10.1007/s00382-020-05438-5

Heo, S., Bell, M. L., & Lee, J.-T. (2019). Comparison of health risks by heat wave definition: Applicability of wet-bulb globe temperature for heat wave criteria. Environmental Research, 168, 158–170. https://doi.org/10.1016/j.envres.2018.09.032

Herman, G. R., & Schumacher, R. S. (2018). Money Doesn't Grow on Trees, but Forecasts Do: Forecasting Extreme Precipitation with Random Forests. Monthly Weather Review, 146(5), 1571–1600. https://doi.org/10.1175/MWR-D-17-0250.1

Hirsch, A. L., Evans, J. P., Di Virgilio, G., Perkins-Kirkpatrick, S. E., Argüeso, D., Pitman, A. J., Carouge, C. C., Kala, J., Andrys, J., Petrelli, P., & Rockel, B. (2019). Amplification of Australian Heatwaves via Local Land-Atmosphere Coupling. Journal of Geophysical Research: Atmospheres, 124(24), 13625–13647. https://doi.org/10.1029/2019JD030665

HITZIGER, S. (2015). Modeling The Variability of Electrical Activity in The Brain, PhD Thesis.

IPCC. (2014): Summary for Policymakers. In: Climate Change 2014: Mitigation of Climate Change. Contribution of Working Group III to the Fifth Assessment Report of the Intergovernmental Panel on Climate Change [Edenhofer, O., R. Pichs-Madruga, Y. Sokona, E. Farahani, S. Kadner, K. Seyboth, A. Adler, I. Baum, S. Brunner, P. Eickemeier, B.

Kriemann, J. Savolainen, S. Schlömer, C. von Stechow, T. Zwickel and J.C. Minx (eds.)]. Cambridge University Press, Cambridge, United Kingdom and New York, NY, USA.

Jacques-Dumas, V., Ragone, F., Borgnat, P., Abry, P., & Bouchet, F. (2022). Deep Learning-based Extreme Heatwave Forecast. Frontiers in Climate, 4, 789641. https://doi.org/10.3389/fclim.2022.789641

Jeff Heaton. (2018). Ian Goodfellow, Yoshua Bengio, and Aaron Courville: Deep learning: The MIT Press, 2016, 800 pp, ISBN: 0262035618. Genetic Programming and Evolvable Machines, 19(1–2), 305–307. https://doi.org/10.1007/s10710-017-9314-z

Johnson, J. M., & Khoshgoftaar, T. M. (2020). The Effects of Data Sampling with Deep Learning and Highly Imbalanced Big Data. Information Systems Frontiers, 22(5), 1113–1131. https://doi.org/10.1007/s10796-020-10022-7

Kiliçarslan, S., Adem, K., & ÇeliK, M. (2021). An overview of the activation functions used in deep learning algorithms. Journal of New Results in Science, 10(3), 75–88. https://doi.org/10.54187/jnrs.1011739

Kober, J., Bagnell, J. A., & Peters, J. (2013). Reinforcement learning in robotics: A survey. The International Journal of Robotics Research, 32(11), 1238–1274. https://doi.org/10.1177/0278364913495721

KOUAKOU, K. A. (2020). Impact of climate change and urbanization on the continental terminal aquifer recharge in aghien lagoon area (abidjan, côte d'ivoire).

Kouassi, A. M. (2021). évolution des normales des pluies extremes en afrique de l'ouest : cas du district d'abidjan (sud de la cote d'ivoire). Agronomie Africaine.

Kurth, T., Treichler, S., Romero, J., Mudigonda, M., Luehr, N., Phillips, E., Mahesh, A., Matheson, M., Deslippe, J., Fatica, M., Prabhat, P., & Houston, M. (2018). Exascale Deep Learning for Climate Analytics. SC18: International Conference for High Performance Computing, Networking, Storage and Analysis, 649–660. https://doi.org/10.1109/SC.2018.00054

Lagerquist, R., McGovern, A., & Gagne Ii, D. J. (2019). Deep Learning for Spatially Explicit Prediction of Synoptic-Scale Fronts. Weather and Forecasting, 34(4), 1137–1160. https://doi.org/10.1175/WAF-D-18-0183.1

Lavaysse, C., Cammalleri, C., Dosio, A., van der Schrier, G., Toreti, A., & Vogt, J. (2018). Towards a monitoring system of temperature extremes in Europe. Natural Hazards and Earth System Sciences, 18(1), 91–104. https://doi.org/10.5194/nhess-18-91-2018

Li, X., Stringer, L. C., & Dallimer, M. (2022). The Impacts of Urbanisation and Climate Change on the Urban Thermal Environment in Africa. Climate, 10(11), 164. https://doi.org/10.3390/cli10110164

Liu, Z., Anderson, B., Yan, K., Dong, W., Liao, H., & Shi, P. (2017). Global and regional changes in exposure to extreme heat and the relative contributions of climate and population change. Scientific Reports, 7(1), 43909. https://doi.org/10.1038/srep43909

Longadge, M. R., Dongre, S. S., & Malik, D. L. (2013). Class Imbalance Problem in Data Mining: Review. 2(1).

Loughnan, M. (2014). Heatwaves are silent killers. Geodate, 27(1), 7-10.

Lu, J., Behbood, V., Hao, P., Zuo, H., Xue, S., & Zhang, G. (2015). Transfer learning using computational intelligence: A survey. Knowledge-Based Systems, 80, 14–23. https://doi.org/10.1016/j.knosys.2015.01.010

Lucas, R. A. I., Epstein, Y., & Kjellstrom, T. (2014). Excessive occupational heat exposure: A significant ergonomic challenge and health risk for current and future workers. Extreme Physiology & Medicine, 3(1), 14. https://doi.org/10.1186/2046-7648-3-14

Madakam, S., Uchiya, T., Mark, S., & Lurie, Y. (2022). Artificial Intelligence, Machine Learning and Deep Learning (Literature: Review and Metrics). Asia-Pacific Journal of Management Research and Innovation, 18(1–2), 7–23. https://doi.org/10.1177/2319510X221136682

McGregor, G. R., Bessemoulin, P., Ebi, K. L., & Menne, B. (Eds.). (2015). Heatwaves and health: Guidance on warning-system development. World Meteorological Organization : World Health Organization.

Meehl, G. A., & Tebaldi, C. (2004). More Intense, More Frequent, and Longer Lasting Heat Waves in the 21st Century. Science, 305(5686), 994–997. https://doi.org/10.1126/science.1098704

Melillo, J. M., Richmond, T. (T. C.), & Yohe, G. W. (2014). Climate Change Impacts in the United States: The Third National Climate Assessment. U.S. Global Change Research Program. https://doi.org/10.7930/J0Z31WJ2

Meyer, L., Brinkman, S., van Kesteren, L., Leprince-Ringuet, N., & van Boxmeer, F. (2015). Technical Support Unit for the Synthesis Report.

Michelozzi, P., Accetta, G., De Sario, M., D'Ippoliti, D., Marino, C., Baccini, M., Biggeri, A., Anderson, H. R., Katsouyanni, K., Ballester, F., Bisanti, L., Cadum, E., Forsberg, B., Forastiere, F., Goodman, P. G., Hojs, A., Kirchmayer, U., Medina, S., Paldy, A., … Perucci, C. A. (2009). High Temperature and Hospitalizations for Cardiovascular and Respiratory Causes in 12 European Cities. American Journal of Respiratory and Critical Care Medicine, 179(5), 383–389. https://doi.org/10.1164/rccm.200802-217OC

Miroslav, K., & Matwin, S. (1997). Addressing the curse of imbalanced training sets: One-sided selection In Icml (Vol. 97, No. 1, p. 179).

Mukhamediev, R. I., Popova, Y., Kuchin, Y., Zaitseva, E., Kalimoldayev, A., Symagulov, A., Levashenko, V., Abdoldina, F., Gopejenko, V., Yakunin, K., Muhamedijeva, E., & Yelis, M. (2022). Review of Artificial Intelligence and Machine Learning Technologies: Classification, Restrictions, Opportunities and Challenges. Mathematics, 10(15), 2552. https://doi.org/10.3390/math10152552

Ngoungue Langue, C. G., Lavaysse, C., Vrac, M., & Flamant, C. (2022). Heat waves monitoring over West African cities: Uncertainties, characterization and recent trends [Preprint]. Atmospheric, Meteorological and Climatological Hazards. https://doi.org/10.5194/nhess-2022-192

Pan, S. J., Kwok, J. T., & Yang, Q. (2008). Transfer Learning via Dimensionality Reduction.

Park, M., Jung, D., Lee, S., & Park, S. (2020). Heatwave Damage Prediction Using Random Forest Model in Korea. Applied Sciences, 10(22), 8237. https://doi.org/10.3390/app10228237

Pascal, M., Wagner, V., Le Tertre, A., Laaidi, K., Honoré, C., Bénichou, F., & Beaudeau, P. (2013). Definition of temperature thresholds: The example of the French heat wave warning system. International Journal of Biometeorology, 57(1), 21–29. https://doi.org/10.1007/s00484-012-0530-1

Perkins, S. E. (2015). A review on the scientific understanding of heatwaves—Their measurement, driving mechanisms, and changes at the global scale. Atmospheric Research, 164–165, 242–267. https://doi.org/10.1016/j.atmosres.2015.05.014

R. G. STEADMAN. (1979). The Assessment of Sultriness. Part I: A Temperature-Humidity Index Based on Human Physiology and Clothing Science.

Rasamoelina, A. D., Adjailia, F., & Sincak, P. (2020). A Review of Activation Function for Artificial Neural Network. 2020 IEEE 18th World Symposium on Applied Machine Intelligence and Informatics (SAMI), 281–286. https://doi.org/10.1109/SAMI48414.2020.9108717

Rasmussen, C. E., & Williams, C. K. I. (2006). Gaussian processes for machine learning. MIT Press.

Ringard J, Dieppois B, Rome S, Dje Kouakou B, Konaté D, Katiellou G. L., Lazoumar R. H., Bouzou-Moussa I, Konaré A, Diawara A, Ochou A.D, Assamoi P, Camara M, Dionguea, Descroix L, & Diedhiou A. (2014). Évolution des pics de températures en afrique de l'ouest: étude comparative entre Abidjan et Niamey.

Rome, S., Pohl, B., Oueslati, B., Moron, V., Raymond, F., Janicot, S., & Diedhou, A. (2019). Durée et fréquence des vagues de chaleur en Afrique tropicale septentrionale selon 5 indices de chaleur.

Rosenblatt, F. (1957). The perceptron, a perceiving and recognizing automaton Project Para. Cornell Aeronautical Laboratory.

Russo, S., Dosio, A., Graversen, R. G., Sillmann, J., Carrao, H., Dunbar, M. B., Singleton, A., Montagna, P., Barbola, P., & Vogt, J. V. (2014). Magnitude of extreme heat waves in present climate and their projection in a warming world. Journal of Geophysical Research: Atmospheres, 119(22). https://doi.org/10.1002/2014JD022098

Shaposhnikov, D., Revich, B., Bellander, T., Bedada, G. B., Bottai, M., Kharkova, T., Kvasha, E., Lezina, E., Lind, T., Semutnikova, E., & Pershagen, G. (2014). Mortality Related to Air Pollution with the Moscow Heat Wave and Wildfire of 2010: Epidemiology, 25(3), 359–364. https://doi.org/10.1097/EDE.0000000000000090

Sherwood, S. C., Huber, M., & Emanuel, K. A. (2010). An adaptability limit to climate change due to heat stress. Proceedings of the National Academy of Sciences of the United States of America, 107(21), 9552–9555.

Shi, Y., Ren, C., Luo, M., Ching, J., Li, X., Bilal, M., Fang, X., & Ren, Z. (2021). Utilizing world urban database and access portal tools (WUDAPT) and machine learning to facilitate spatial estimation of heatwave patterns. Urban Climate, 36, 100797. https://doi.org/10.1016/j.uclim.2021.100797

Smith, T. T., Zaitchik, B. F., & Gohlke, J. M. (2013). Heat waves in the United States: Definitions, patterns and trends. Climatic Change, 118(3–4), 811–825. https://doi.org/10.1007/s10584-012-0659-2

Snoek, J., Larochelle, H., & Adams, R. P. (2012). Practical Bayesian Optimization of Machine Learning Algorithms.

Stafoggia, M., Forastiere, F., Agostini, D., Biggeri, A., Bisanti, L., Cadum, E., Caranci, N., de??Donato, F., De Lisio, S., De Maria, M., Michelozzi, P., Miglio, R., Pandolfi, P., Picciotto, S., Rognoni, M., Russo, A., Scarnato, C., & Perucci, C. A. (2006). Vulnerability to Heat-Related Mortality: A Multicity, Population-Based, Case-Crossover Analysis. Epidemiology, 17(3), 315–323. https://doi.org/10.1097/01.ede.0000208477.36665.34

Staudemeyer, R. C., & Morris, E. R. (2019). Understanding LSTM -- a tutorial into Long Short-Term Memory Recurrent Neural Networks (arXiv:1909.09586). arXiv. http://arxiv.org/abs/1909.09586

Stillman, J. H. (2019). Heat Waves, the New Normal: Summertime Temperature Extremes Will Impact Animals, Ecosystems, and Human Communities. Physiology, 34(2), 86–100. https://doi.org/10.1152/physiol.00040.2018

Stull, R. (2011). Wet-Bulb Temperature from Relative Humidity and Air Temperature. Journal of Applied Meteorology and Climatology, 50(11), 2267–2269. https://doi.org/10.1175/JAMC-D-11-0143.1

Sung, T.-I., Wu, P.-C., Lung, S.-C., Lin, C.-Y., Chen, M.-J., & Su, H.-J. (2013). Relationship between heat index and mortality of 6 major cities in Taiwan. Science of The Total Environment, 442, 275–281. https://doi.org/10.1016/j.scitotenv.2012.09.068

Sylla, M. B., Nikiema, P. M., Gibba, P., Kebe, I., & Klutse, N. A. B. (2016). Climate Change over West Africa: Recent Trends and Future Projections. In J. A. Yaro & J. Hesselberg (Eds.), Adaptation to Climate Change and Variability in Rural West Africa (pp. 25–40). Springer International Publishing. https://doi.org/10.1007/978-3-319-31499-0_3

Sylvain Gnamien. (2022). Caracterisation de la pollution particulaire (PM10 ET PM2.5) a Abidjan et Korhogo (Cote d'Ivoire) en lien avec la santé des populations. Ingénierie de l'environnement.

Takahashi, K., Honda, Y., & Emori, S. (2007). Assessing Mortality Risk from Heat Stress due to Global Warming. Journal of Risk Research, 10(3), 339–354. https://doi.org/10.1080/13669870701217375

Taylor, M. E., & Stone, P. (2009). Transfer Learning for Reinforcement Learning Domains: A Survey.

Tetens. (1930). Uber einige meteorologische Begriffe.

Torrey, L., & Shavlik, J. (2010). Transfer learning. In Handbook of research on machine learning applications and trends: Algorithms, methods, and techniques (pp. 242–264). IGI Global.

Tong, S., FitzGerald, G., Wang, X.-Y., Aitken, P., Tippett, V., Chen, D., Wang, X., & Guo, Y. (2015). Exploration of the health risk-based definition for heatwave: A multi-city study. Environmental Research, 142, 696–702. https://doi.org/10.1016/j.envres.2015.09.009

Tong, S., Wang, X. Y., & Barnett, A. G. (2010). Assessment of Heat-Related Health Impacts in Brisbane, Australia: Comparison of Different Heatwave Definitions. PLoS ONE, 5(8), e12155. https://doi.org/10.1371/journal.pone.0012155

Wang, L. (2016). Discovering Phase Transitions with Unsupervised Learning. Physical Review B, 94(19), 195105. https://doi.org/10.1103/PhysRevB.94.195105

Xu, Z., FitzGerald, G., Guo, Y., Jalaludin, B., & Tong, S. (2016). Impact of heatwave on mortality under different heatwave definitions: A systematic review and meta-analysis. Environment International, 89–90, 193–203. https://doi.org/10.1016/j.envint.2016.02.007

Ymba, M. (2022). Analyse des effets des îlots de chaleur urbains sur la santé des populations de la ville d'Abidjan (Côte d'Ivoire).

Yu, S., Tett, S. F. B., Freychet, N., & Yan, Z. (2021). Changes in regional wet heatwave in Eurasia during summer (1979–2017). Environmental Research Letters, 16(6), 064094. https://doi.org/10.1088/1748-9326/ac0745

Zhu, Y., Chen, Y., Lu, Z., Pan, S., Xue, G.-R., Yu, Y., & Yang, Q. (2011). Heterogeneous Transfer Learning for Image Classification. Proceedings of the AAAI Conference on Artificial Intelligence, 25(1), 1304–1309. https://doi.org/10.1609/aaai.v25i1.8090

Table of Contents